3D-PRINTED LITHIUM-ION-SIEVE ADSORBENTS FOR LITHIUM RECOVERY FROM Li-ION BATTERY METALS RECYCLING PROCESS RAFFINATES

Lappeenranta–Lahti University of Technology LUT

Master's programme in Chemical Engineering for Energy Transition, Master's thesis

2026

Sami Hartikainen

Examiners: Associate Professor Sami Virolainen, D.Sc.

Post-doctoral Researcher Youssef El Ouardi, PhD.

ABSTRACT

Lappeenranta–Lahti University of Technology LUT

LUT School of Engineering Sciences

Chemical Engineering

Sami Hartikainen

3D-PRINTED LITHIUM-ION-SIEVE ADSORBENTS FOR LITHIUM RECOVERY FROM Li-ION BATTERY RECYCLING PROCESS RAFFINATES

Master's thesis in Chemical Engineering

2026

70 pages, 22 figures, and 14 tables

Examiners: Associate Professor Sami Virolainen, D.Sc. and Youssef El Ouardi, PhD.

Keywords: Lithium; 3D printed adsorbent; Ion sieve; Battery recycling; Battery raffinate; Adsorption

Lithium is used widely in batteries to power various electronic devices. A sharp increase in demand is being driven by the increasing production of consumer electronics, and more recently, the production of electric vehicles and grid battery storages. The rising number of end-of-life batteries has resulted in the emergence of recycling processes for the recovery of various valuable metals including lithium from them. However, the recovery of lithium in these processes is often incomplete, leaving behind a battery raffinate with lithium contents of 1400 – 2000 mg/L, with a sodium to lithium ratio of 10 – 100. The recovery of the remaining lithium is challenging due to both its low concentration, which limits the effectiveness of precipitation, and the significantly higher sodium content present in the raffinate.

The purpose of this thesis was to develop a highly selective and 3D-printable adsorbent for the recovery of lithium from raffinates. Ion sieves are specialized inorganic adsorbents, which usually consist of manganese or titanium oxides to achieve good performance or a more dissolution-resistant structure respectively. In this thesis, a combined titanium-manganese ion sieve adsorbent is synthesized and 3D-printed with the purpose of achieving competitive performance with a resistant structure.

The results show the synthesized adsorbent to be extremely selective for lithium, while also providing improved dissolution resistance compared to manganese-based ion sieves. The adsorption process was shown to prefer high pH values, and to be highly endothermic, with large increases in performance achieved in temperature-controlled column application.

TIIVISTELMÄ

Lappeenrannan–Lahden teknillinen yliopisto LUT

LUTin insinööritieteiden tiedekunta

Kemiantekniikka

Sami Hartikainen

3D-TULOSTETUT LITIUM-IONISEULA ADSORBENTIT LITIUMIN TALTEENOTTOON Li-ION AKKUJEN KIERRÄTYSPROSESSIEN RAFFINAATEISTA

Kemiantekniikan diplomityö

2026

70 sivua, 22 kuvaa, ja 14 taulukkoa

Tarkastajat: Tutkijaopettaja Sami Virolainen, D.Sc. ja Tutkijatohtori Youssef El Ouardi, PhD.

Avainsanat: Litium; 3D tulostettu adsorbentti; Ioniseula; Akkujen kierrätys; Akkujen raffinaatti; Adsorptio

Litiumia käytetään laajasti akuissa erilaisten elektronisien laitteiden virtalähteinä. Jyrkkä kasvu kysynnässä johtuu kulutuselektroniikan kasvavasta tuotannosta sekä viimeaikoina myös sähköautojen ja sähköverkkojen akkuvarastoista. Jatkuvasti kasvava elinkaarensa loppuun kuluneiden akkujen määrä on johtanut kierrätysprosessien syntymiseen, joiden tarkoituksena on erilaisten arvokkaiden metallien, mukaanlukien litiumin talteenotto. Litiumin talteenotto näissä prosesseissa on kuitenkin usein epätäydellistä, ja jäljelle jää akkuraffinaatti, jonka litiumpitoisuus on 1400 – 2000 mg/L, jossa natriumia on 10 – 100 kertainen määrä litiumin suhteen. Jäljelläolevan litiumin talteenotto on haastavaa alhaisen konsentraation vuoksi, joka rajoittaa saostamisen tehokkuutta, sekä raffinaatin suuren natriumkonsentraation vuoksi.

Tämän diplomityön tarkoitus oli kehittää erittäin selektiivinen ja 3D-tulostettava adsorbentti litiumin talteenottoon raffinaateista. Ioniseulat ovat epäorgaanisia adsorbentteja, jotka koostuvat usein mangaani- tai titaanioksideista, joilla vastaavasti saavutetaan joko hyvä suorituskyky tai liukenemista kestävä rakenne. Tässä diplomityössä syntesoitiin yhdistetty titaani-mangaani ioniseula, joka pystytään 3D-tulostamaan tarkoituksena saavuttaa hyvä suorituskyky kestävän rakenteen kanssa.

Tulokset osoittavat syntesoidun adsorbentin olevan erittäin selektiivinen litiumille, saavuttaen samalla paremman kemiallisen kestävyyden mangaanipohjaisiin ioniseuloihin verrattuna. Adsorptioprosessin osoitettiin suosivan korkeita pH-arvoja, ja se oli erittäin endoterminen, jolloin suorituskyky parani huomattavasti lämpötilaa nostattaessa kolonniadsorptiossa.

ACKNOWLEDGEMENTS

I want to thank my examiners, Sami Virolainen and Youssef El Ouardi for giving me this opportunity to work on something so completely new and interesting to me, I learned a lot during these 6 months. I want to give additional thanks to Youssef for his guidance in my activities during this thesis work. I also want to thank researchers Ekaterina Bandina and Kosisochi Ibebunjo for their guidance on how to use the 3D-printer, and also for their invaluable assistance as I was troubleshooting my problems with it.

Finally, I wish to thank my friends and family for being there with me for all these years, with special thanks to my father, who has always been there to support me no matter what.

SYMBOLS AND ABBREVIATIONS

Roman characters

$\%R$	Removal percentage	%
c_0	Initial concentration	mg/L
c_e	Equilibrium concentration	mg/L
V	Volume	m^3
m	Mass	kg
K	Selectivity coefficient	
$q_e(a)$	Adsorption capacity of desired ion	mg/g
$q_e(b)$	Adsorption capacity of competing ion	mg/g
$c_e(a)$	Equilibrium concentration of desired ion	mg/L
$c_e(b)$	Equilibrium concentration of competing ion	mg/L
T	Temperature	ºC, K
K_F	Freundlich exponent	mg/g
n	Freundlich constant	
K_L	Langmuir constant	L/mg
Q_m	Maximum adsorption capacity	mg/g

Abbreviations

LIB	Lithium-Ion Battery
LIS	Lithium Ion Sieve
LMO	Lithium Manganese Oxide
LTO	Lithium Titanium Oxide
LTMO	Lithium Titanium Manganese Oxide
3D	Three dimensional
CAD	Computer Assisted Design
FDM	Fused Deposition Modelling
SLA	Stereolithography
SLS	Selective Laser Sintering
PA12	Polyamide 12
FTIR	Fourier-Transform Infrared Spectroscopy
ATR	Attenuated Total Reflectance
XRD	X-Ray Diffraction
AAS	Atomic Adsorption Spectroscopy
SEM	Scanning Electron Microscope

Table of contents

Abstract

Acknowledgements

Symbols and abbreviations

Declarations

1 Introduction 10
2 Lithium 12
2.1 Production 12
2.2 Applications 15
2.3 Recycling and circular economy 16
3 Processes for recycling spent Li-ion batteries 17
3.1 Pretreatment 18
3.2 Leaching 20
3.3 Purification and metal recovery 22
3.4 Adsorption 25
4 Ion sieves 27
4.1 Manganese ion sieves 27
4.2 Titanium ion sieves 29
4.3 Synthesis of lithium-ion sieves 30
4.4 Properties and applications 32
5 3D-printing technology 33
5.1 Fused Deposition Modelling (FDM) 34
5.2 Stereolithography (SLA) 35
5.3 Selective Laser Sintering (SLS) 37
5.3.1 Principle 37
5.3.2 Applications 39
6 Materials and methods 41
6.1 Chemicals 41

6.2 Preparation of powder LTMO adsorbents 41
6.3 Powder batch sorption experiments 42
6.4 Characterization of LTMO 43
6.5 Preparation of 3D-printed adsorbents 43
6.6 3D-print sorption experiments 44
6.6.1 Batch 45
6.6.2 Column 45
7 Results and discussion 46
7.1 Materials characterization 46
7.2 Batch sorption with powders 49
7.3 Sorption experiment with 3D-printed adsorbents 51
7.3.1 Batch sorption 51
7.3.2 Effect of temperature in batch sorption 53
7.3.3 Chemical stability 54
7.3.4 Column sorption 55
7.3.5 Effect of temperature in column sorption 57
7.4 Sorption performance of similar ion-sieves 58
7.5 Challenges of ion-sieve sorbents 60
8 Conclusions 61
References 63

DECLARATIONS

Turnitin

The originality of this thesis has been reviewed with the Turnitin similarity checking service.

AI usage

The author of this thesis, Sami Hartikainen, did not use any AI tools during the preparation of the thesis**.**

Responsibility

The author, Sami Hartikainen, takes full responsibility for the content of this thesis and has reviewed and edited the content generated by the possible use of AI tools.

1 Introduction

Lithium is a critical component of lithium-ion batteries (LIBs), which are present in numerous electronic devices today. In 2011, lithium was mainly used as a structural reinforcement material in glass and ceramics. However, the rapid rise in consumer demand for electronic devices and vehicles has resulted in batteries gaining an 87 % share of all lithium use in 2024 (*U.S. Mineral Commodity Summaries,* 2024). Lithium demand has been increasing at an 18 % annual rate, and it is estimated that if similar year-on-year increases in lithium demand continue, current reserves could be depleted within 25 years (Bae & Kim, 2021). This has contributed to an increased research interest in the recycling of LIBs, as less than 1 % of lithium is recycled currently (Bae & Kim, 2021). The recycling of LIBs is challenging, as they come in various sizes, shapes, and have different inherent cell chemistries. Therefore, a single process for recycling all LIBs does not exist, leading to the use of different methods and technologies. The hydrometallurgical recycling method, which consists of pretreatment, acid leaching, and a recovery method such as precipitation, solvent exchange or ion exchange, is often favoured. This method offers various benefits, such as easier scalability, lower energy consumption and fewer carbon emissions compared to pyrometallurgy, while also being suitable for different cell chemistries (Kaczorowska, 2024; Neumann et al., 2022). Research is focusing on improving various aspects of the recycling process, such as by substituting inorganic acids for organic acids to achieve less harmful gas emissions and less acidic wastewaters (Yao et al., 2018).

Even after hydrometallurgical recovery of metals from the LIB leachate through precipitation, solvent exchange or ion exchange, considerable amounts of lithium remain in the spent lithium-ion battery raffinate. In fact, the lithium concentrations in the raffinate can exceed those found in conventional lithium brine recovery sites, resulting in an incentive to retrieve lithium from the raffinate (Li, X. et al., 2025). The use of selective inorganic adsorbents, known as ion sieves, have been extensively studied for the recovery of lithium from various aqueous solutions. However, most research has focused mostly on lithium recovery from brines and seawater. Ion sieves are typically composed of lithium manganese oxides (LMO) or lithium titanium oxides (LTO), with studies aiming to improve their synthesis and performance. Manganese-based sieves are characterized by their improved adsorption performance in comparison to titanium-based sieves, although their structure is

prone to dissolution under acidic conditions. In contrast, titanium-based sieves are structurally stable and acid resistant, although their adsorption performance is comparatively lower (Weng, D. et al., 2020; Xu, X. et al., 2016).

The goal of this thesis is to design and develop a selective lithium adsorbent material to be used for lithium adsorption from battery raffinates. This material will used as an additive to a structural material and will be 3D-printed into 3D adsorbent units. As much research has been done on titanium and manganese -based ion sieves, there is interest in a combined, titanium-manganese based sieve to combine the strengths of both materials. While very little research has been conducted on combined titanium-manganese ion sieves in powdered form, this thesis focuses how this material may be 3D-printed, and how it affects the adsorption performance and selectivity of the material. The experimental work of this thesis focuses on what are the optimal parameters for materials synthesis, 3D-printing, and adsorption conditions to achieve high adsorption capacities in combination with the exceptional selectivity inherent to ion sieves.

2 Lithium

Lithium is a soft, silvery and shiny alkali metal with the atomic number 3, and among the alkali metals, it has the highest melting point at 181 °C and the highest boiling point at 1330 °C. The density of lithium is 0.534 g/cm^3, making it the lightest of all metals (Sicius, 2024). Due to its nature as an alkali metal, lithium is highly reactive, with reactions with water, organics and fluorocarbons being the most violent (Tabares, 2013). Lithium is favoured as a battery material due to three main benefits: its high reactivity due to readily losing its outermost electron is important in facilitating the flow of current within batteries. It is much lighter than other battery metals, such as lead or nickel. Lastly, due to its high reactivity, a lot of energy can be stored in its atomic bonds. As a result of these benefits, lithium-ion batteries have higher cell voltages and much higher energy densities than alternative batteries, while also taking up less space and materials to manufacture (Arote, 2022).

Due to its high reactivity, lithium doesn't occur in its elemental form in nature. Lithium is present in almost all igneous rocks, with estimations placing the lithium content of the earth's crust at around 60 mg/L (Sicius, 2024). Lithium is also present in spring waters, oceans, and brines, with the lithium content of seawater estimated at 0.18 mg/L. Many brines have lithium contents at hundreds of mg/L, while a few have been confirmed to have lithium contents of more than 1000 mg/L (Meng et al., 2021).

2.1 Production

Estimates from 2023 place the amount of lithium reserves in the world at 26000 kt, with the two main raw material sources for lithium production being brines and ores. The largest brine reservoirs are in Chile, with a size of 9200 kt, and the largest ore reserves are located in Australia, sizing 4700 kt. The lithium content in brines results from the leaching of volcanic rocks, and much of the brine-based production is concentrated in various salt flats across South America. Spodumene is the most common commercially mined and refined lithium containing ore, with Australia recently becoming the leader in spodumene mining. Developments in the extraction and processing of lepidolite, another type of lithium ore, have been carried out in China recently. (IEA, 2024; Marcinov et al., 2023). The

development of world lithium production from 2010 to 2023 is shown in Figure 1, and the major lithium producing countries are shown in Figure 2.

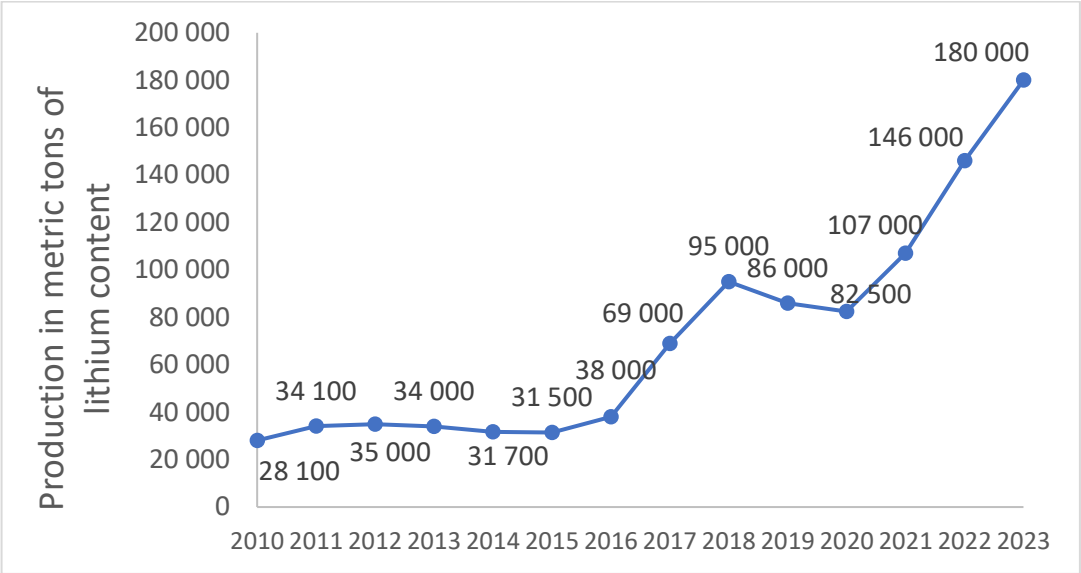

Figure 1. World lithium production from 2010 to 2023 (US Geological Survey & Statista, 2024b)

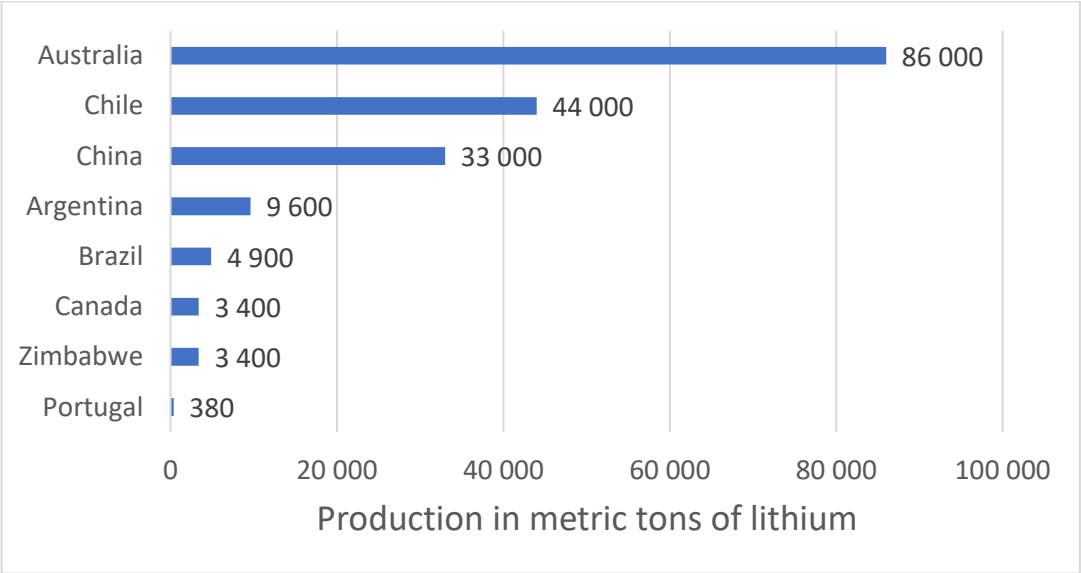

Figure 2. Major lithium producing countries worldwide in 2023 (US Geological Survey & Statista, 2024a)

The largest lithium producers in the world are Australia, Chile and China, with brine-based production from Argentina and Brazil following behind (Marcinov et al., 2023; US Geological Survey & Statista, 2024a) Total global lithium production in 2023 was approximately 180000 t, with Australia contributing 86000 t. Salt flats in Chile produced

44000 t, while China has increased its production efforts to 33000 t (US Geological Survey & Statista, 2024a). Out of all global production, 54 % of lithium is produced from ores and minerals, while 46 % is produced from brines (OECD, 2024).

While lithium production is spread out across different continents, China holds a majority share of 57 % in lithium refining. As the largest consumer and refiner of lithium, China has relied on imports to meet domestic industry demand, mostly from Australian spodumene mines. Recent developments in China have resulted in ramping up domestic production in the form of salt brines and newly developed lepidolite mines, with estimations indicating that China could surpass Chile in production during this decade (IEA, 2024).

The main process for lithium recovery from brines is the soda evaporation process consisting of several steps: evaporation, impurity removal, and precipitation using carbonation. Salt brines around the world differ in chemistry and composition, and therefore recovery processes vary slightly based on site, but the main steps and objectives are similar. Dry and sunny climates are advantageous for production, because they accelerate the very slow evaporation process, and lithium recovery from brine is still approximately 30 – 50% cheaper than production from ores (Meng et al., 2021).

Up to 90 % of non-brine-based lithium production comes from spodumene ore. After crushing and upgrading through flotation, the ore in its α-spodumene form is roasted or calcined at 1100 °C to convert it into β-spodumene, which is less resistant to various leaching chemicals (Marcinov et al., 2023; Meng et al., 2021). After this, there are three different pathways for processing spodumene: acid, alkaline and chlorination processes. The acid process consists of further crushing and treating the β-spodumene with H_2SO_4 at 250 °C. The ore can then be leached with a leaching solution, and once impurities are removed, the lithium is carbonated to produce lithium carbonate (Li_2CO_3). The alkaline process starts with limestone or soda ash treatment to convert lithium into a soluble form, which then reacts with carbon dioxide. After impurity removal, the solution is evaporated to form lithium crystals. In the chlorination process, the ore is treated with chlorine compounds, such as hydrochloric acid, sodium chloride, or chlorine gas, the selection of which depends on the nature of the mineral. Chlorination results in lithium chloride (LiCl), which is then water-leached and purified (Meng et al., 2021).

2.2 Applications

The share of applications for lithium has changed drastically in recent years. Lithium is used in a variety of industries; it is mainly used in LIBs but is also used in the production of high-temperature lubricating greases, and flux powders for metal casting. Until relatively recently, the main use for lithium was in ceramics and glass, where it acted as a structural enhancer for ceramics and as an additive to glass, increasing the melt rate while decreasing viscosity. (Bae & Kim, 2021; Meng et al., 2021). Lithium salts are used in lithium therapy to treat mental disorders (Sicius, 2024). Growing markets utilizing LIBs include many small portable electronic devices and electronic tools, as well as larger products such as grid-scale energy storage systems and electronic vehicles (*U.S. Mineral Commodity Summaries,* 2024).

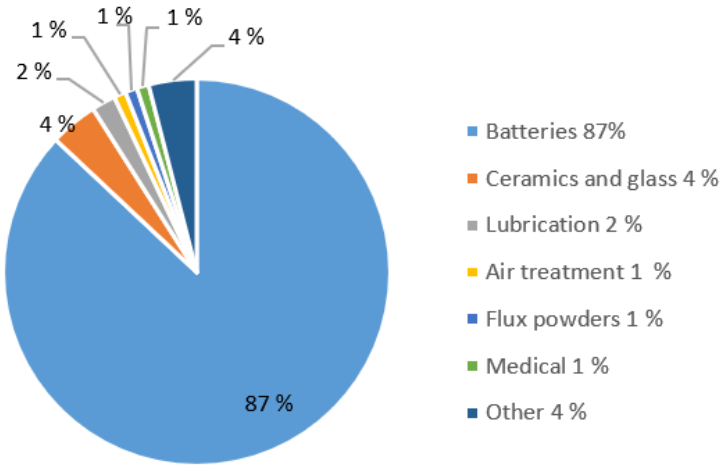

Figure 3. Global end-use cases for lithium in 2024 (*U.S. Mineral Commodity Summaries,* 2024).

Figure 3 shows the end-use cases for lithium in 2024, with batteries being by far the largest, and this has been the driving force behind recent increases in lithium demand (Meng et al., 2021). Lithium is a desirable material in battery production due to its special properties. It is not only the lightest metal, but it also has the highest electrochemical potential and the highest energy density of all metals. LIBs in many consumer electronic devices, such as phones and laptops, require only a couple grams or up to a couple of dozen grams of lithium to manufacture. On the other hand, electric vehicle batteries take around 20 kg of lithium, while energy storage system batteries require hundreds or thousands of kilograms depending on their size (Bae & Kim, 2021). However, LIBs have not always been the dominant lithium

product on the market. In 2011, the largest use case for lithium was in glass and ceramics with a 30 % share of lithium use, followed by batteries. In 2019, batteries accounted for a majority share of all lithium consumption at 65 %, driven by the increasing demand for electronic devices and the growing electric vehicle markets (Bae & Kim, 2021).

2.3 Recycling and circular economy

Due to the increase in demand of LIBs, recycling processes focused on recovering lithium and other precious metals from spent batteries has gained significant interest. From 2018 to 2019, the number of electric vehicles in the world increased by 64 %, reaching 5.6 million units (Baum et al., 2022). At the same time, total lithium consumption increased by 18 %, with estimations showing that current lithium reserves will be depleted in 25 years (Bae & Kim, 2021). Currently, less than 1 % of lithium is recycled (Bae & Kim, 2021), while the amount of LIB waste keeps growing every year. It is estimated that electric vehicles produced in 2019 will result in 500000 tons of LIB waste at the end of their lifespan, and this is estimated to increase to 8 million tons by 2040 (Baum et al., 2022).

Various challenges exist in setting up the necessary infrastructure for the collection of LIBs for recycling. There is a wide variety of LIBs on the market, with varying sizes and cell chemistries (Neumann et al., 2022). Not all recycling methods are economically viable or even suitable for all cell chemistries (Neumann et al., 2022), and some methods are much more effective in separating specific metals (Baum et al., 2022). Therefore, special attention must be paid in sorting waste LIBs and choosing suitable recycling methods (Neumann et al., 2022).

3 Processes for recycling spent Li-ion batteries

Various pyrometallurgical, electrochemical and hydrometallurgical processes are available for the recycling of LIBs. Among these methods, hydrometallurgical processes are often preferred due to their advantages in scalability, low operating temperature, low energy consumption, low CO_2 emissions (Kaczorowska, 2024; Li, X. et al., 2025), and compatibility with different cell chemistries and types (Colledani et al., 2023; Thompson et al., 2020).

Pyrometallurgical methods rely on turning the metal oxides in battery materials into metals by utilizing heat. These methods usually only require a few simple pretreatment steps and can be suitable for various types of LIBs. However, not all pyrometallurgical methods are suitable for recovering lithium, and they instead focus on other valuable metals such as cobalt. Currently many recycling facilities utilize pyrometallurgy or a combination of pyro- and hydrometallurgy in their recycling processes, with the largest facility capable of processing 100000 tons of waste per year utilizing this combination. In contrast, the majority of methods in development focus on hydrometallurgy, due to lower implementation costs in comparison to pyrometallurgy (Baum et al., 2022).

However, hydrometallurgical recycling processes require proper pre-treatment of batteries to ensure efficient metal recovery, and the reagents used during the recycling process can be costly (Colledani et al., 2023). Leaching with large volumes of acid is the most commonly used method for LIB recycling, which results in a spent Li-rich raffinate after metal extraction. This raffinate still contains large amounts of sodium and lithium, with lithium concentrations between 1400 – 2000 mg/L, and a sodium to lithium ratio between 10 – 100 (Li, J. et al., 2025). As the lithium content is higher than most conventional brine recovery sites, this serves as an incentive to develop specific recovery methods for these raffinates (Li, X. et al., 2025).

Hydrometallurgical processes excel at treating ores and materials with low concentrations of metals and are therefore suitable for the recovery of various metals from wastes and secondary raw materials, such as LIBs. Hydrometallurgical processes rely on using aqueous solutions of acids or bases to dissolve metals from materials and then recover them utilizing recovery processes, such as precipitation or electrowinning (Virolainen, 2013).

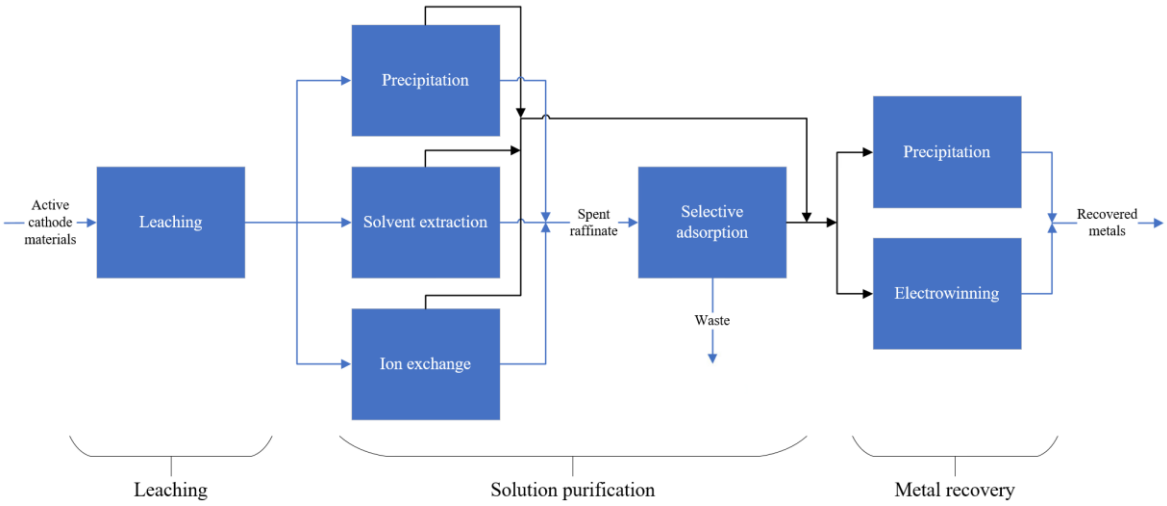

Figure 4. Block diagram of potential steps in a hydrometallurgical LIB recycling process.

Typical hydrometallurgical recycling processes for LIBs consist of three main steps after pre-treatment: leaching, solution purification, and metal recovery, which are shown in Figure 4. Solution purification is carried out either by precipitation, solvent extraction, or ion-exchange. A combination of several purification methods is often used in recycling processes (Neumann et al., 2022). Due to the specified high amount of lithium still present in spent LIB raffinate after metal recovery, a refined metal extraction approach employing novel Li-3D-printed monolithic ion exchanger adsorbents (a form of ion-exchange) will be studied. The final step in the process is metal recovery, which is often performed by precipitation or electrowinning. Many of the valuable metals can be recovered as precipitates (Yao et al. 2018), but cobalt is often recovered by electrowinning, and the method is applicable for nickel as well (Huang et al., 2018; Łacinnik et al., 2025).

3.1 Pretreatment

LIBs are made up of various chemicals and materials, resulting in a complex structure and chemical composition. Therefore, pretreatment of batteries prior to recycling is essential to separate aluminium and copper foils and cathode active materials, which contain Li, Co, Ni, and Mn, from other components, such as casings, anodes, electrolytes, and electrical systems (Xu, Z. et al., 2023; Yao et al., 2018). The quality of the pretreatment process directly affects the energy consumption, profitability, and efficiency of the following recycling and recovery processes (Xu, Z. et al., 2023). Various technologies exist for LIB pretreatment, but the

general process consists of three main steps: discharging, dismantling, and separation of materials containing precious metals (Li, L. et al., 2024; Xu, Z. et al., 2023; Yao et al., 2018).

Discharging is the first and most important step in ensuring the safety of the recycling process. It reduces the possibility of LIBs self-igniting or short circuiting, which could lead to cell explosions later in the process (Colledani et al., 2023; Li, L. et al., 2024; Yao et al., 2018). Even when the battery is discharged to 0 % state of charge, it still retains a residual voltage, which must be permanently eliminated through irreversibly over-discharging (Colledani et al., 2023).

LIBs may be discharged physically by short circuiting the electrodes; however, this releases a large amount of heat, making constant cooling necessary. In comparison to physical discharging, chemical discharging has gained interest in research due to its ease of use and suitability for all battery types (Xu, Z. et al., 2023). Chemical discharging involves immersing LIBs in salt solutions such as NaCl or $FeSO_4$, which absorb the remaining charge from the battery (Li, L. et al., 2024; Yao et al., 2018).

Discharged batteries will be dismantled into different parts either manually or mechanically. Manual separation involves the use of hand tools and is not suitable for large scale recycling processes due to the large number of batteries to be recycled (Yao et al., 2018) and the slowness of the process (Xu, Z. et al., 2023). A mechanical dismantling process, which consists of crushing, sieving and separating materials with machinery is often favoured because of its high efficiency and automation (Dong et al., 2025; Yao et al., 2018). Utilizing sieving alongside crushing can efficiently separate more valuable materials such as electrode powder, cobalt and lithium from casing materials. After crushing, iron containing casing materials and various copper and aluminium foils were found to have larger and rougher particle sizes than cobalt and lithium, which facilitates their mechanical separation (Li, L. et al., 2024).

Electrode materials in LIBs are adhered to current collectors in aluminium foils with binders such as polyvinylidene fluoride. The active materials may be separated either by dissolving the binder material or by applying a thermal treatment process (Dong et al., 2025; Yao et al., 2018). The binder materials can be dissolved with solvents, such as N-methylpyrrolidone, allowing for the recovery of the electrode materials and the aluminium foil in its metal form. However, this method is not widely applied at a large scale, because despite the potential for

solvent reuse, they are expensive, and different solvents may be required for various battery types depending on the polarity of the binder material (Yao et al., 2018). In a thermal treatment process, organic materials are burnt off in a furnace, resulting in a simple and highly efficient process suitable for large scale application (Dong et al., 2025; Yao et al., 2018). Nevertheless, combustion inherently releases emissions of smoke and toxic gases (Yao et al., 2018).

3.2 Leaching

Leaching is the extraction of metals from solid materials into liquid by converting them into soluble ions. Common leaching agents include water, various organic and inorganic acids, and bases. In addition, various oxidizing and reducing agents can be utilized to increase the efficiency of leaching by changing the oxidation state of metal ions to a state that is more soluble in leaching solutions. In the case of LIBs, the active cathode materials are leached for their valuable metals utilizing acids (Virolainen, 2013; Yao et al., 2018).

Inorganic acids are the most commonly utilized leaching agents, with research showing recovery efficiencies of over 99 % being possible for inorganic acids (Neumann et al., 2022). The most commonly used inorganic acids are sulfuric acid (H_2SO_4), hydrochloric acid (HCl), and nitric acid (HNO_3) (Dong et al., 2025; Neumann et al., 2022; Yao et al., 2018). Out of these, H_2SO_4 is preferred due to its lower cost, high leaching effectiveness and compatibility with metal separation methods and the materials of industrial equipment. When leaching LIBs, H_2SO_4 and HCl are exhibit similar leaching effectiveness, while HNO_3 is typically less efficient (Neumann et al., 2022). However, inorganic acids come with drawbacks. HCl contributes process equipment corrosion, increasing maintenance costs (Dong et al., 2025; Li, L. et al., 2024). Additionally, the leaching process using inorganic acids produces gases harmful to the environment and human health, such as NO_x, Cl_2 and SO_x, necessitating purification equipment, which increases both capital and operating costs (Velazquez & Muhr, 2025; Yao et al., 2018). Furthermore, the reusability of inorganic acids as leaching agents is low (Li, L. et al., 2024), and the process generates large amounts of wastewater containing strong acids. These wastewaters pose environmental risks and require dedicated treatment before disposal. Due to these factors, while initial capital costs for a recycling

process utilizing inorganic acids are low, long-term maintenance and operating costs can be high, particularly as the process ages (Li, L. et al., 2024; Yao et al., 2018).

Inorganic acids, especially H_2SO_4 and HNO_3, are commonly used alongside reducing agents, such as hydrogen peroxide (H_2O_2), sodium bisulfite ($NaHSO_3$), glucose (Yao et al., 2018), or biomass (Meshram et al., 2016). The reducing agents function by converting higher oxidation states of metal ions present in LIBs, such as Co^{3+} and Mn^{4+}, to their divalent states of Co^{2+} and Mn^{2+}. These divalent metal ions are much more soluble in acidic leaching solutions than their higher valence counterparts (Meshram et al., 2016; Yao et al., 2018). The presence of a reducing agent during leaching with inorganic acids is crucial to achieving maximum recovery efficiency of metal ions (Neumann et al., 2022), and certain reducing agents, such as H_2O_2 can also accelerate the leaching rate of the process (Yao et al., 2018). In a study by Meshram et al. (2016), utilizing 1 M H_2SO_4 for leaching LIBs resulted in recoveries of 93.4 % for lithium, 66.2 % for cobalt, 96.3 % for nickel and 50.2 % for manganese. When 5 % H_2O_2 was introduced as a reducing agent cobalt recovery increased to 79.2 % and manganese recovery to 84.6 %. The use of 0.78 % $NaHSO_3$ resulted in even greater recovery rates across the board, with 96.7 % lithium, 91.6 % cobalt, 96.4 % nickel, and 87.9 % manganese being recovered.

Due to the challenges of using inorganic acids, recent research interest has focused on the utilization of organic acids in leaching. Studies have shown that leaching LIBs with organic acids can achieve recovery rates averaging around 99 %, but rates of almost 100 % have also been achieved for lithium. While many organic acids have demonstrated these high recovery rates, they typically require the presence of reducing agents (Neumann et al., 2022; Yao et al., 2018), even though many organic acids exhibit both leaching and reducing properties simultaneously (Li, L. et al., 2024). Studied organic acids for LIB leaching include succinic, ascorbic, citric, malonic and malic acid among others (Neumann et al., 2022; Yao et al., 2018). Studies have shown that certain organic acids to have specific beneficial properties. For example, leaching LIBs with oxalic acid produces lithium and cobalt oxalates, which can be selectively separated due to their difference in solubility. Meanwhile, malonic acid forms stable complexes with metal ions, which greatly increases its leaching effectiveness compared to other acids (Dong et al., 2025). In fact, the extraction mechanism of many organic acids consists of two parts: metal ion solubilization in acid solutions and complexation with organic acids (Li, L. et al., 2024).

Table 1. Advantages and disadvantages of different leaching techniques.

Method	Advantages	Disadvantages
Inorganic acid leaching	- Very high efficiency - Good compatibility with separation methods - H_2SO_4 is cost-effective	- Leads to equipment corrosion - Produces harmful NO_x, Cl_2 and SO_x emissions - Generates strong acid containing wastewater - Low reusability
Organic acid leaching	- High efficiencies with reducing agents - Operates under milder leaching conditions - Better reusability - Causes less equipment corrosion - Emits fewer harmful gases - Forms chelating bonds with lithium	- Higher operating costs - Slower leaching rates

As shown in table 1, organic acids offer several advantages over inorganic acids, such as milder leaching conditions, better recyclability, lower emission of hazardous gases (Yao et al., 2018), and less corrosion to equipment (Li, L. et al., 2024). In lithium extraction from LIBs, organic acids effectively form strong chelating bonds with lithium. These strong bonds involving many molecular forces enable organic acids to achieve leaching performance similar to strong inorganic acids in a much milder and less acidic environment (Li, L. et al., 2024). Given these advantageous properties, research is increasingly focused on replacing inorganic acids with organic acids for LIB leaching. However, their commercial application is hindered by higher costs, higher operating costs, and slower leaching rates (Velazquez & Muhr, 2025).

3.3 Purification and metal recovery

After leaching, valuable metals must be separated, purified, and recovered from the pregnant leach solution. Precipitation is an essential hydrometallurgical method that involves adding a precipitant into the solution, causing metals to react and form insoluble compounds, usually

in the form of metal hydroxides, sulfides or carbonates (Velazquez & Muhr, 2025). The solubility of these compounds is highly dependent on pH, thus, monitoring and adjusting pH is the main method of controlling the process (Virolainen, 2013).

In a typical LIB recycling process, the most common separation steps include precipitation of Fe, Al and Cu as impurities, solvent extraction of Mn, Co and Ni, and the precipitation of lithium (Neumann et al., 2022). Although various methods exist for precipitating the valuable metals in LIBs, the complexity of the leaching solutions due to the large amount of battery types with different structures and chemistries often necessitates the use of multiple different precipitation steps to achieve optimal metal recovery (Yao et al., 2018). Common precipitation methods for metals found in LIBs is shown in table 2.

Table 2. Commonly available precipitation methods for valuable metals present in LIBs. Compiled from Yao et al. (2018).

Metal	Precipitant	pH	Precipitate	Reference
Li	Na_2CO_3	10	Li_2CO_3	(Zhu et al., 2012)
Co	NaOH	11–12	$Co(OH)_2$	(Shuva & ASW, 2013)
	$(NH_4)_2C_2O_4$	2	CoC_2O_4	(Zhu et al., 2012)
Ni	Na_2CO_3	9	$NiCO_3$	(Meshram et al., 2015)
Mn	Na_2CO_3	7.5	$MnCO_3$	(Meshram et al., 2015)
Cu	Na_2S	1	CuS	(Kang et al., 2010)
	NaOH	6.45–6.5	$Cu(OH)_2$	(Gratz et al., 2014)
Al	NaOH	3.5	$Al(OH)_3$	(Weng, Y. et al., 2013)
Co, Ni, Mn Coprecipitation	$H_2C_2O_4$	-	$Ni_xCo_yMn_{1-x-y}C_2O_4$	(Zhang, X. et al., 2018)
	NaOH	9–11	$Ni_xCo_yMn_{1-x-y}(OH)_2$	(Sandhya et al., 2016)
	Na_2CO_3	7.5	$Ni_xCo_yMn_{1-x-y}CO_3$	(He et al., 2018)

Separating Co, Ni and Mn completely from a leach solution is difficult due to the chemical similarity of these metals and usually requires complex and expensive separation processes with multiple steps (He et al., 2018). In order to reduce the required number of steps (Yao et al., 2018) and lower precipitation costs (He et al., 2018), a strategy involving the coprecipitation of multiple metals is used. The goal of coprecipitation is the direct synthesis of the cathode material $LiNi_{1/3}Co_{1/3}Mn_{1/3}O_2$, which is commonly used in commercial LIBs (He et al., 2018). As shown in table 2, Co, Ni, and Mn are usually coprecipitated in the form $Ni_xCo_yMn_{1-x-y}(OH)_2$ using NaOH, or as $Ni_xCo_yMn_{1-x-y}CO_3$ using Na_2CO_3 or as $Ni_xCo_yMn_{1-}$

$_{x-y}C_2O_4$ using $H_2C_2O_4$ as the precipitant. The cathode materials are acquired by reacting Li_2CO_3 with the precipitates (Yao et al., 2018).

While table 2 shows that many valuable metals can be successfully recovered as precipitates, electrowinning can be utilized for the recovery of Co and Ni (Huang et al., 2018; Łacinnik et al., 2025). In most commercial recycling processes, Co is already recovered by electrowinning, while the recovery of Ni is seeing growing interest in research (Łacinnik et al., 2025). Electrowinning is an electrochemical method, where an electrical current is used to deposit metal ions from a solution onto the surface of an anode, allowing for the recovery of metals with high purity (Huang et al., 2018; Łacinnik et al., 2025).

Lithium is commonly recovered with precipitation as Li_2CO_3 or Li_3PO_4, with common precipitants for lithium recovery being Na_2CO_3 and Na_3PO_4 with CO_2 also providing a more sustainable alternative for lithium precipitation (Velazquez & Muhr, 2025). Among these options, precipitation to Li_2CO_3 is favoured as it is easier to achieve, more economical, and more efficient than alternative choices (Bae & Kim, 2021), and providing higher achievable purities from precipitation (Velazquez & Muhr, 2025).

The efficiency of lithium carbonate precipitation is affected by both temperature and the pH of the solution (Neumann et al., 2022). Specifically, lithium carbonate is inverse soluble, with high temperatures decreasing solubility and improving precipitation yields. An alternative precipitant for lithium carbonate is CO_2, where carbonation is driven by the dissolution of CO_2 and the resulting formation of bicarbonate. This process is also highly dependent on temperature and an alkaline pH, so maintaining high pH levels is crucial. Although using CO_2 is more sustainable, the precipitation yields are usually relatively low (Velazquez & Muhr, 2025).

While lithium precipitation to Li_2CO_3 is an economical choice that can also provide high purity yields, low concentrations of lithium remain in the solutions. Therefore, Li_2CO_3 precipitation should be combined with other recovery methods to maximize lithium recovery (Velazquez & Muhr, 2025).

3.4 Adsorption

Adsorption is the adhesion of atoms, ions, biomolecules or molecules from a gas, liquid or dissolved solid onto a surface. While many intermediary cases exist, adsorption is classified into two types: physical adsorption (physisorption) and chemical sorption (chemisorption) (Ruthven, 1984). Most used adsorbents are solids, so the adsorption process usually takes place at a solid-gas or solid-liquid interface, with other phase combinations being applied at an experimental level (Dabrowski, 2001).

Table 3. Differences between physisorption and chemisorption (Ruthven, 1984).

Physisorption	**Chemisorption**
- Low heat of adsorption	- High heat of adsorption
- Non-specific	- Highly specific
- No dissociation of adsorbed species	- May involve dissociation
- Non-activated, rapid and reversible	- Activated, may be slow and irreversible
- No electron transfer	- Electron transfer resulting in bond formation

Table 3 shows the general features of both physisorption and chemisorption. The heat of adsorption is the heat energy released as the adsorbate binds to the adsorbent surface, and it is a direct measure of the strength of the bonding between them. Physisorption involves weak intermolecular forces including van der Waals forces and electrostatic interactions such as polarization and dipole interactions. Chemisorption involves the formation of chemical bonds between a sorbent molecule and the adsorbent surface. Chemisorption, unlike physisorption, requires activation energy to occur, and the process is often irreversible (Ruthven, 1984).

The performance of adsorbents can be quantified with adsorption experiments by calculating the removal efficiency (%R) or adsorption capacity (q_e) (Tangkas et al., 2023). The selectivity of adsorbents is important when dealing with solutions containing competing ions. In a binary system, the selectivity coefficient K may be calculated once the adsorption capacities and equilibrium concentrations are known.

$$\%R = \frac{c_0 - c_e}{c_0} \cdot 100\ \% \quad (1)$$

$$q_e = \frac{(c_0 - c_e) \cdot V}{m} \quad (2)$$

Where c_0 is initial concentration, c_e is equilibrium concentration, V is volume of adsorbate solution, and m is mass of adsorbent (Tangkas et al., 2023).

$$K = \frac{q_e(a)/c_e(a)}{q_e(b)/c_e(b)} \quad (3)$$

Where $q_e(a)$ is the capacity for of the ion of interest (lithium), $q_e(b)$ is the capacity of the competing ion (sodium), $c_e(a)$ is the equilibrium concentration of the ion of interest, and $c_e(b)$ is the equilibrium concentration of the competing ion (Tangkas et al., 2023).

While utilizing adsorption for spent battery raffinate, it is important for adsorbents to be selective specifically for lithium, so that the adsorbent performance isn't hindered by the large amount of sodium and other competing metals present in the raffinate.

4 Ion sieves

The development of new adsorbents has become a key research focus, primarily aimed at creating materials with enhanced selectivity, higher adsorption capacity, and improved thermal, chemical and mechanical stability, along with an improved lifespan.

Ion sieves, a class of selective adsorbents, are frequently used for lithium extraction from primary sources, such as brines, due to their affordability and ease of application. Lithium ion-sieves (LIS) provide excellent selectivity for lithium even in the presence of various impurities and competing ions due to their chemical and microscopical structures (Chen et al., 2024). Specifically, LISs possess cavities of the appropriate size for lithium ions, and since lithium is the smallest metal ion, competing ions are unable to fit within the structure of the LIS. Titanium and manganese are used for LISs in the form of lithium manganese oxides (LMO) and lithium titanium oxides (LTO), with LMO usually having higher performance in capacity and selectivity, while LTO have more stable structures (Weng, D. et al., 2020; Xu, X. et al., 2016). Previous studies have demonstrated the use of LISs for lithium extraction from batteries, with manganese-based LISs proving to be an effective but relatively expensive method (Bae & Kim, 2021).

Studies on LISs have shown them to be effective for lithium recovery from battery raffinates, with manganese-based LISs outperforming aluminium-based adsorbents (Li, X. et al., 2025). However, manganese-based LISs tend to suffer from material loss during adsorption and desorption cycles, while aluminium-based adsorbents exhibit less material loss via dissolution (Kaczorowska, 2024; Li, X. et al., 2025). Titanium-based LISs have more stable structures than manganese-based counterparts, and therefore experience less material loss during dissolution, but their adsorption performance is weaker (Kaczorowska, 2024; Weng, D. et al., 2020).

4.1 Manganese ion sieves

Manganese-based ion sieves are derived from synthesizing lithium containing LMOs from precursor lithium and manganese salts. The precursor salts are combined, usually through a solid synthesis method, into a mixture that is then calcined to form the LMO product. The

LMO is then eluted with acid to replace the Li^+ ions present in the lattice structure with H^+ ions, transforming it into a protonated form commonly referred to as HMO. The protonated HMO is capable of adsorbing lithium by replacing the H^+ ions present in the lattice.

Only a few LMO type LISs capable of reaching high lithium adsorption capacities have been synthesized, which include λ-MnO_2, $MnO_2 \cdot 0.3H_2O$ and $MnO_2 \cdot 0.5H_2O$, which are derived from $LiMn_2O_4$, $Li_{1.33}Mn_{1.67}O_4$ ($Li_4Mn_5O_{12}$) and $Li_{1.6}Mn_{1.6}O_4$ ($Li_2Mn_2O_5$) respectively (Chen et al., 2024; Weng, D. et al., 2020; Xu, X. et al., 2016). The adsorption capacity of LMOs is dependent on the Li/Mn molar ratio of the material, with a higher ratio generally resulting in higher adsorption capacities (Xu, X. et al., 2016). As such, of the manganese-based ion sieves, $MnO_2 \cdot 0.5H_2O$ currently has the highest potential adsorption capacity of 72.9 mg/g (Li et al., 2023) due to a Li/Mn molar ratio of 1:1 resulting from the $Li_{1.6}Mn_{1.6}O_4$ material (Chen et al., 2024; Weng, D. et al., 2020). LMO type LISs are characterized by their high adsorption capacity, excellent regeneration performance and high selectivity (Weng, D. et al., 2020). While the LMO type LIS is widely utilized due to its advantages, it suffers from manganese dissolution in aqueous solutions (Xu, X. et al., 2016). During the exchange of lithium and hydrogen ions in an acidic solution, manganese forms Mn^{4+} and Mn^{2+} ions in the LMO structure. While Mn^{4+} is stable in the structure, Mn^{2+} is prone to dissolving in the acid solution. Over time, this dissolution can deteriorate the structure of the LMO, which impacts its recyclability and adsorption capacity (Chen et al., 2024).

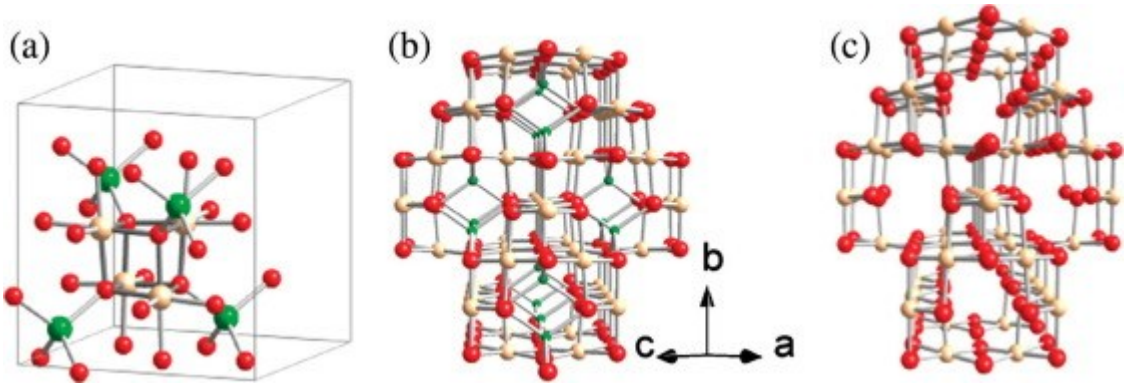

Figure 5. Structure of (a) a cubane core of spinel $LiMn_2O_4$, (b) extended 3D framework of $LiMn_2O_4$, and (c) extended 3D framework of $LiMn_2O_4$ with lithium ions removed, showing vacant sites. (Green spheres represent lithium, red spheres represent oxygen, and beige spheres represent manganese). (Xu, X. et al., 2016)

All synthesized LMOs exhibit spinel structures, such as those shown in Figure 5, which contribute to their selective adsorption performance (Xu, X. et al., 2016). The spinel structure is a cubic crystal arrangement, in which lithium ions occupy tetrahedral sites, manganese ions occupy octahedral sites, and oxygen anions occupy face-centered cubic sites (Chen et al., 2024; Weng, D. et al., 2020). The selective adsorption performance is facilitated by channels within the structure, allowing Li^+ to move freely and intercalate within the spinel lattice of the LMO (Weng, D. et al., 2020).

4.2 Titanium ion sieves

The synthesis process for titanium-based ion sieves is similar to that of LMOs, but the manganese salt precursor is substituted for a titanium salt. After synthesis the lithium containing LTO are also eluted with acid to form HTO. Currently two primary types of LTOs exist, these being H_2TiO_3 eluted from synthesized Li_2TiO_3, and $H_4Ti_5O_{12}$ from synthesized $Li_4Ti_5O_{12}$ (Chen et al., 2024; Xu, X. et al., 2016) The LTO derived from Li_2TiO_3 is characterized by a layered crystal structure, with cubic close packed oxygen atoms and metal atoms in octahedral voids. In the structure shown in Figure 6, Li and Ti form two different types of layers, one consisting of only Li atoms and the other layer consisting of $LiTi_2$, with both atoms in their stoichiometric amounts. The $Li_4Ti_5O_{12}$ sieves exhibit a spinel structure similar to that of LMOs, but they have a better cycling performance than their manganese counterparts due to the stronger Ti–O bond (Xu, X. et al., 2016).

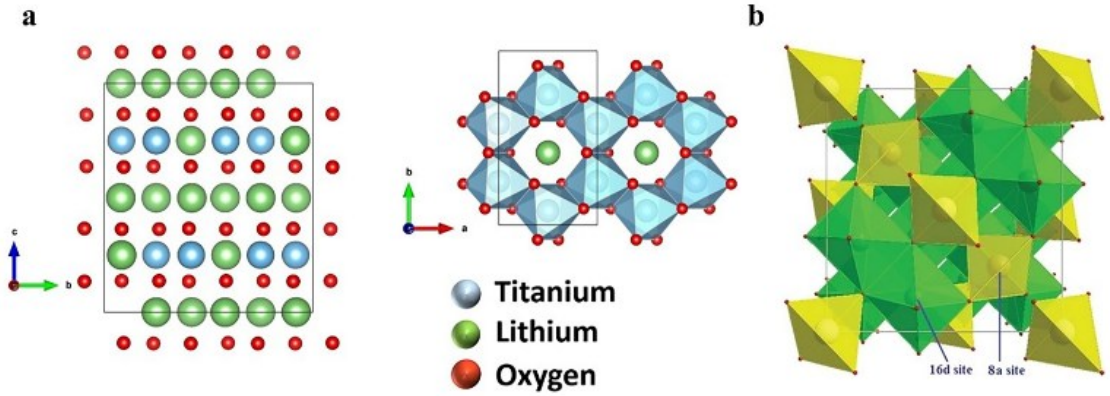

Figure 6. Crystal structure of (a) layered Li_2TiO_3 and honeycomb-like TiO_6 structure in $LiTi_2$ layers, and (b) spinel $Li_4Ti_5O_{12}$ (yellow tetrahedra represent lithium, and green octahedra represent disordered lithium and titanium) (Marthi et al., 2021; Sun et al., 2015).

In comparison to LMOs, LTOs are less prone to dissolution losses in acidic solutions. Their main advantages over LMOs include a more stable structure and better acid resistance, which results in extremely low dissolution of Ti. Their performance as an adsorbent remains stable, even after multiple adsorption/desorption cycles (Chen et al., 2024). However, LTOs do not perform well in aqueous solutions under electrical currents (Xu, X. et al., 2016). Advantages and disadvantages of LMO and LTO type sieves are summarized in table 3.

Table 3. Advantages and disadvantages of LMO and LTO type ion sieves.

Ion sieve type	Advantages	Disadvantages
LMO	- High adsorption capacity - Excellent regeneration performance - High selectivity - Compatible with electrochemical methods	- Manganese loss during adsorption/desorption cycle
LTO	- Acid-resistant structure - Stable adsorption performance - High selectivity	- Worse adsorption performance than LMO - Non-functional under electrical currents

4.3 Synthesis of lithium-ion sieves

LISs are generally prepared by synthesising lithium-containing powders, which are then eluted with acid. Common synthesis methods including the sol-gel process, hydrothermal methods, and solid-state reactions (Kaczorowska, 2024; Martínez et al., 2024). Microwave assisted methods have also been studied to reduce synthesis times and energy consumption (Martínez et al., 2024).

Solid-state reactions are the most used method for the synthesis of LISs due to their relative simplicity and low cost of the method, as well as the fact that they do not require the usage of solvents (Tangkas et al., 2023). This method involves mechanically mixing lithium salts with the desired titanium or manganese salt, followed by calcination of the mixture at high temperatures (Xu, X. et al., 2016).

In the sol-gel process, soluble lithium, manganese, or titanium compounds are dispersed in a colloidal solution also called ‘sol’. The solution undergoes mixing to form a wet gel, which is then dried and subsequently calcined to form the desired LMO or LTO (Xu, X. et al., 2016; Zhang, L. et al., 2016). The sol-gel process allows for the synthesis of highly homogenous and pure LIS powders (Xu, X. et al., 2016).

The hydrothermal method involves the synthesis of crystals in an aqueous solution placed in a closed system at high temperatures and pressures (Byrappa & Yoshimura, 2013). In this process, lithium hydroxide is mixed with metal salts and calcined. The calcined material is then mixed with an aqueous lithium hydroxide solution, and undergoes hydrothermal synthesis (Wang et al., 2016). This method is typically performed in autoclaves at temperatures above 100 °C, with synthesis processes lasting up to several days (Ranjbar et al., 2014; Wang et al., 2016).

Several studies have investigated the synthesis, properties, and applications of LISs, with a particular focus on their use for lithium recovery from saltwater brines. Yu et al., (2023) developed a titanium-based 3D-printed LIS by first preparing a LIS slurry, which was then 3D-printed using an extrusion printing process and calcined at temperatures between 300–600 °C. While the adsorption capacity of the 3D-printed LIS was roughly 18.4 % worse than powdered LIS, it achieved similar performance in selectivity for lithium, and the adsorption capacity was stable after several adsorption/desorption cycles. In addition, the 3D-printed monolithic structure resulted in high compressive strength making it durable and suitable for industrial application while also extending the life cycle of the adsorbent.

An LMO sieve with the formula $Li_{1.33}Mn_{1.67}O_4$ was prepared with solid state reactions by Li, X. et al. (2025), by using a mortar to mechanically mix $MnCO_3$ and Li_2CO_3 to achieve the desired Li:Mn molar ratio, and the mixture was then calcined at 500 °C. The LMO was compared to an aluminium-based adsorbent and was found to be more efficient.

Since LMOs provide better performance but suffer from material dissolution, while LTOs provide good structural stability, researchers have explored combining these properties. Ryu, et al. (2019) prepared various Lithium Titanium Manganese Oxide (LTMO) sieves with the formula $Li_{1.33}(Ti_xMn_{1-x})_{1.67}O_4$, varying the Ti:Mn ratio (x). The synthesis was performed by a solid-state process, mechanically mixing Li_2CO_3, $MnCO_3$ and TiO_2 with a ball mill, and the mixtures were calcined at temperatures between 500–900 °C. The best performing

LTMO composition $Li_{1.33}(Ti_{0.1}Mn_{0.9})_{1.67}O_4$ (x = 0.1) was obtained at 500 °C. This LTMO showed significantly lower Mn dissolution in acid compared to LMO-based sieves.

4.4 Properties and applications

The specific selectivity effect of LISs is based on their crystal structure. As synthesised LMO, LTO and LTMO materials are eluted with acid to facilitate ion exchange, the Li^+ ions in the structure are replaced with H^+ ions, resulting in HMO, HTO, and HTMO adsorbents (Kaczorowska, 2024).

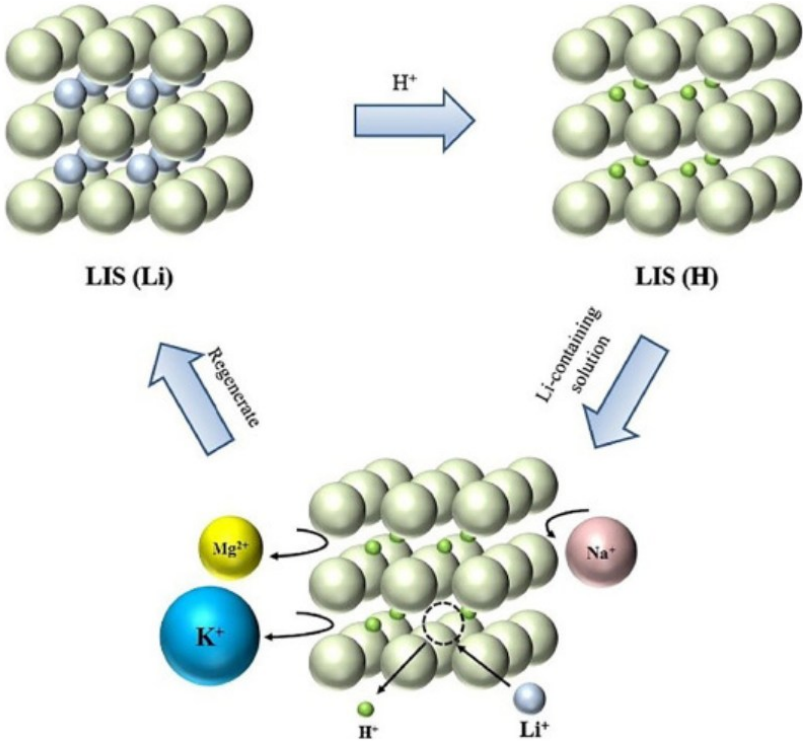

Figure 7. Representation of the selective adsorption process of LISs (Xu, X. et al., 2016).

Due to the stability of the crystal structure, the removed Li^+ ions result in vacant crystal sites, sized to accommodate the ions. As shown in Figure 7, when the eluted LIS filled with H^+ ions is exposed to a solution containing lithium and other metal ions, these vacant crystal sites are preferentially reoccupied by lithium. As lithium possesses the smallest ionic radius, it is favored over other metal ions, which are less able to fit into the available crystal sites, resulting in the high degree of selectivity in adsorption. This phenomenon is commonly known as the "ion-sieve effect" or "LIS effect". (Chen et al., 2024; Weng, D. et al., 2020; Xu, X. et al., 2016).

LISs are primarily utilized for the selective separation of lithium from aqueous solutions, including sewage, brines, and waste leachates (Kaczorowska, 2024). Their application has gained significant research attention, particularly for the extraction of lithium from seawater and salt brines. Conventional separation methods, such as solar evaporation, solvent extraction, and co-precipitation are either extremely time consuming or have very limiting operating conditions. Furthermore, these processes also lead to severe environmental pollution and can even cause corrosion of processing equipment. In comparison, LIS technology offers high separation efficiency and high purity lithium products, while eliminating the need for additional purification process steps and being less toxic to the environment (Weng, D. et al., 2020; Xu, X. et al., 2016). However, industrial application is hindered by manganese pollution resulting from the dissolution of LMO-based sieves, and challenges with the powder forming process (Xu, X. et al., 2016).

5 3D-printing technology

3D printing, also known as additive manufacturing or layered manufacturing, is the process of creating 3-dimensional objects from model data generated with 3D Computer Aided Design (CAD) programs. The fabrication process after model generation is automatic and performed by adding material layer by layer in powder, solid, or liquid form depending on the printing technology used (Natarajan et al., 2021). Utilization of 3D printing technology is often split into two categories of application: rapid prototyping and rapid manufacturing. Rapid prototyping applications include producing concept models of a prototype product, or functional prototypes, where certain functions such as moving or connecting parts can be demonstrated and iterated on. Rapid manufacturing involves fabricating parts of a product or a complete final product to be used directly after manufacturing (Gebhardt et al., 2019).

The 3D printing process consists of different steps, beginning with the creation of a 3D CAD model of the desired object or by imaging an object with Computerized Tomography (CT) scanning. The model is then sliced using specialized software, converting it into several horizontal layers with uniform thickness, after which the 3D printing machine collects the information on contour data, thickness and the number of layers. The 3D printer utilizes the information to convert the 3D model into physical layers, generating a tool path for the 3D

printing tool. The actual fabrication process begins with the machine printing the lowest layer of the object and printing successive connected layers on top of each other until the object is fully printed (Gebhardt et al., 2019; Kumar, 2020).

Various 3D printing technologies exist to utilize different materials for fabrication. Objects can be made from metals, polymers, ceramics, or composite materials by utilizing corresponding material powders, slurries or filaments. The American Society for Testing and Materials (ASTM) has issued a standard classifying 3D printing processes into seven different categories: Binder jetting, Directed energy deposition, Material extrusion, Material jetting, Powder bed fusion, Sheet lamination and Vat photopolymerization (Kumar, 2020).

5.1 Fused Deposition Modelling (FDM)

Fused Deposition Modelling (FDM) is a material extrusion 3D printing process method, which works by partially melting filament, which is usually a thermoplastic, and pushing it through an extruder to build the layers of the printed object. FDM is a registered trademark of the company Stratasys, so filament-based 3D printing technologies are sometimes referred to with the general term Fused Filament Fabrication (FFF) (Godec et al., 2022). FDM is the most widely used 3D printing technology, when considering the number of printers in use. It is an affordable, compact technology, making it popular in the consumer market (Davim & Dave, 2021).

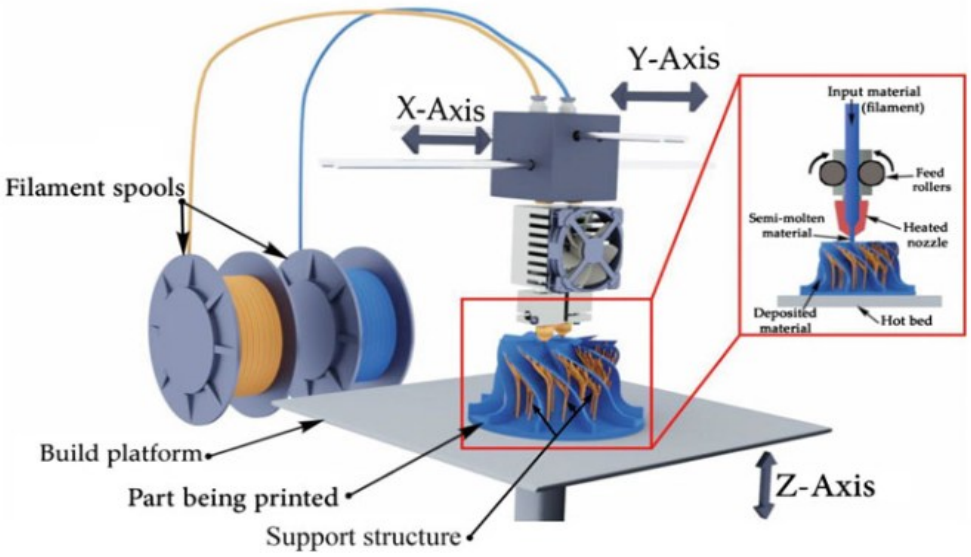

Figure 8. Schematic of FDM printer function (Davim & Dave, 2021).

Figure 8 shows the functional schematic of FDM printers. As the filament is partially melted in the heated nozzle of the extruder, it will be pushed out by the following solid filament. This places restrictions on material choice, as the filament must be strong enough to push the extruded filament but also simplifies extruder design since there is no need for a specific machine part to extrude the partially molten filament. The printed object is fabricated by moving the extruder in the X- and Y-axes and as a layer is completed, the extruder moves in the Z-axis by the layer thickness specified in the design model. As a new layer of filament is extruded on a previous layer, the heat from the extruder partially melts the layer below it, enabling the fusion of the two layers. Depending on the design of the printed object, support structures may be required to help support and shape the partially molten filament. After the printing is completed, these support structures are removed (Davim & Dave, 2021). FDM 3D-printing results in a rough surface for the object, and the process is usually slower and more inaccurate (lower resolution) than other alternative technologies (Godec et al., 2022).

The most used thermoplastic filaments for FDM are acrylonitrile butadiene styrene and poly lactic acid, since they are affordable and usable in simple commercial FDM printers. More expensive high performance and engineering grade thermoplastics are also available and may be reinforced into composites with various materials such as carbon fibre, kevlar or metal powder (Davim & Dave, 2021; Godec et al., 2022).

5.2 Stereolithography (SLA)

Stereolithography (SLA) is a vat photopolymerization technology for 3D-printing, relying on photopolymer materials that solidify under the exposure of a focused ultraviolet laser (Godec et al., 2022). The liquid prepolymer material consisting of monomers and oligomers, is mixed with small organic photoinitiator molecules, which will introduce free radicals or ions into the liquid prepolymer under the exposure of the laser. These free radicals or ions start a chain reaction that polymerizes the liquid material into a solid form in the area of the laser (Bártolo, 2011; Godec et al., 2022). A schematic of SLA printing is shown in Figure 9.

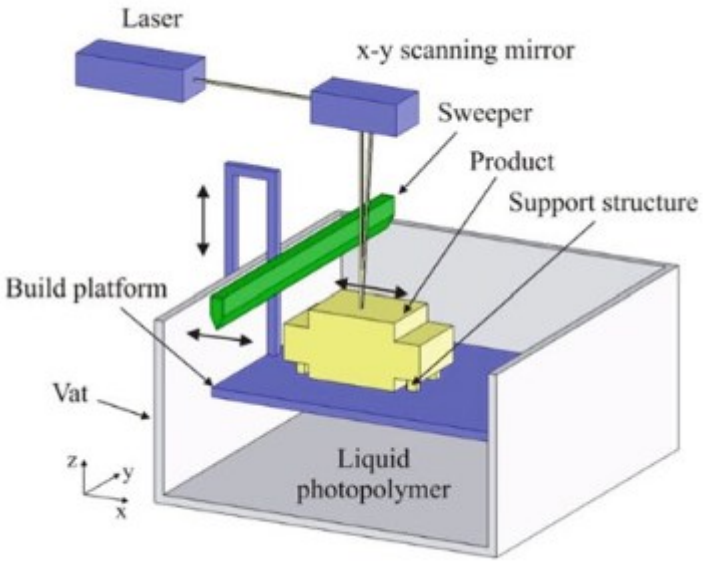

Figure 9. Schematic of SLA function (Godec et al., 2022).

SLA works by focusing ultraviolet light from either a helium-cadmium or argon laser onto the liquid photopolymer contained in the vat (Godec et al., 2022). Alternatives to conventional ultraviolet stereolithography also exist in the form of infrared stereolithography and stereo-thermal-lithography utilizing ultraviolet and infrared (Bártolo, 2011). Polymerization of the liquid photopolymer is done in layers, with the build platform starting just below the surface of the liquid and moving downwards as each layer is finished. A scanning mirror points the laser in the X- and Y-coordinate directions, while the sweeper ensures that no air bubbles are present in the solidifying object. After fabrication is complete, the object is washed from any excess polymer and support structures are removed, after which the object is left to cure for at least an hour to ensure any liquid remaining within the object will polymerize (Godec et al., 2022).

SLA is the oldest 3D-printing technology and it's characterized by its speed and ability to fabricate objects with fine details in high quality. SLA compatible materials are however limited to only expensive photopolymers, which also need to be stored properly to prevent light from causing the polymerization of material before printing. Photopolymers are also known to release harmful gases (Godec et al., 2022).

5.3 Selective Laser Sintering (SLS)

Selective Laser Sintering (SLS) is a powder bed fusion 3D-printing technology utilizing rapid heating from a laser to fuse powdered materials into solid objects. Various different solid and gas lasing mediums (laser sources) are used to produce the laser for SLS. Solid mediums, such as ruby, glass or Ti-sapphire utilize wavelengths between 694 – 2940 nm, while gaseous laser wavelengths have a range of 191 – 10600 nm (Natarajan et al., 2021). The most common lasing medium is a gaseous CO_2 laser operating at 10600 nm (Godec et al., 2022). Some other available gas lasing mediums include some noble gases and their fluorides, such as krypton, argon, ArF and XeF. Metal vapours from copper and gold are also utilized (Natarajan et al., 2021).

5.3.1 Principle

In addition to the laser, the SLS system consists of galvo mirror scanners which orient the laser beam by deflecting it into the correct position (Godec et al., 2022). The build chamber can be placed in an inert atmosphere of Ar or N_2 to prevent oxidation, and the build platform is moved in the Z-axis as each layer of powder is sintered. New powder is deposited from a feed container and spread out in 20 – 150 μm thick layers by a roller or scraper, depending on the machine (Kruth et al., 2005). A schematic of an SLS 3D-printer build chamber and laser is shown in Figure 10.

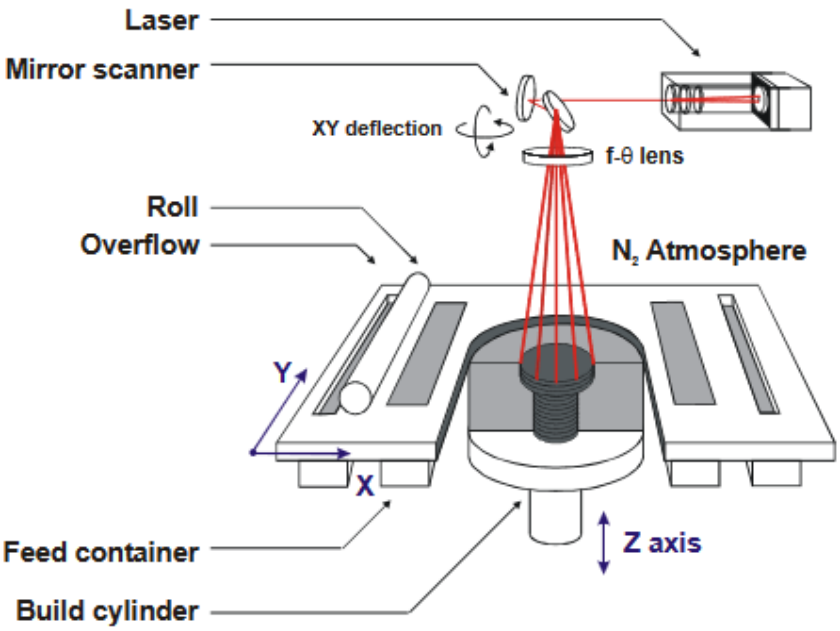

Figure 10. Schematic of SLS machine layout (Kruth et al., 2005).

The manufacturing process begins by optionally inertizing the atmosphere in the build chamber and turning on heaters. Temperature in the chamber is increased to around 12 – 16 °C below the melting point of the powder material, and the rest of the thermal energy needed for melting the powder is provided by the laser. During the heating period, a thin 10 – 12 mm high bed of powder is usually created on the build platform to prevent curling of sintered objects (Godec et al., 2022). As the laser beam heats the powder, it melts either completely or partially, fusing them together. The heat also sinters the new powder layer into the previously sintered layer below it (Natarajan et al., 2021).

After manufacturing is complete, the system and printed objects within must be cooled down naturally over time. Rapid cooling of the system can result in objects being damaged through deformations and distortions. Leftover powder in the build chamber can be reused, though powder close to the sintered object is partially affected by the heat of the laser and should be mixed with fresh powder to ensure the quality of future prints (Godec et al., 2022).

A variety of materials can be used with SLS, such as waxes, ceramics, polymers, metals and metal alloys (Tiwari et al., 2015). Metals and alloys rarely see use with SLS, as they are more often used with selective laser melting technologies. The most used materials in SLS printing are polyamides, namely nylon 11, 12 and 6 (Godec et al., 2022), as they provide excellent strength, fatigue resistance and chemical resistance (Tiwari et al., 2015).

5.3.2 Applications

SLS as a 3D printing method is accurate and allows for design of complex shapes and small geometries while eliminating the need for support structures, as the bed of unsintered powder supports the printed object from all sides. SLS also allows for the fabrication of multiple smaller objects in one run, or the fabrication of large objects. (Godec et al., 2022).

SLS 3D printing provides a high amount of control over the structure of the printed object. By altering machine parameters such as laser power, speed and temperature, the energy density of the laser can be customized, resulting in a solid structure when material is completely molten, and a porous structure when only partially molten. More porous structures naturally allow for a higher degree of permeability for solvents, and objects can be printed with different porosities in the same structure, for example a porous inner structure with a solid outer wall (Lahtinen, 2019).

Research on SLS 3D printing application has been done in various industries. In the medicinal and pharmaceutical field, different SLS printed disintegrating, immediate-release and controlled-release tablets loaded with pharmaceuticals have been developed. Research has shown that the SLS 3D printing process did not cause damage to the pharmaceutical powders. In the medicinal field, personalized implants and dental prosthetics have been printed with SLS (Awad et al., 2020). The effect of SLS printed components in the automotive and aviation industry and have shown promise in lowering energy consumption in both manufacturing of parts and in the use of parts through lowered weights (Hettesheimer et al., 2018).

In studies conducted by Lahtinen (2019), the potential of SLS 3D printed modules for metal separation from printed circuit board leachate containing various metals such as gold, palladium, platinum, copper and iron was examined. The process of material preparation for printing was described, a structure providing host polymer material can be simply mixed with additives that provide necessary chemical functionality. Plain Polyamide 12 (PA12) powder and a 3D printed PA12 filter were demonstrated to be very selective for gold, while observing that the SLS printing process did not damage the adsorptive performance of the material.

For selective adsorption with additives, Lahtinen (2019) utilized chemically inert and stable polypropylene powder as structural material, which was mixed with an anion exchange resin Dowex 21K as an additive. The prepared mixture contained 10 w-% resin, and once printed into a filter it was demonstrated to selectively adsorb 96 % of palladium and 98 % of platinum. A considerable amount of tin, zinc and lead was also adsorbed, resulting in the need for selective elution separation. The porous 3D-printed structures allow for high flow rates of adsorbate fluids, while still affecting the flow so that it increases the contact between the fluid and the active adsorbent materials, facilitating improved mass transfer onto the adsorbent. Importantly, the function and feasibility of selective SLS 3D-printed adsorption modules was demonstrated, and that selectivity can be controlled by mixing in chemically active additives with structural printing powders. The results from these studies make SLS an excellent choice for combining a structural material with LTMO powders as an active material for the 3D-printing of novel ion sieve adsorbent units.

A comparison table consisting of advantages and disadvantages for each presented 3D-printing technology is presented in table 4.

Table 4. Advantages and disadvantages of 3D-printing technologies

Technology	Advantages	Disadvantages
FDM	- Affordable systems - Compact - Easy to use, even at consumer level - Materials can be reinforced to various composites	- Slow - Rough surfaces - Low resolution
SLA	- High resolution with fine details - Printing of transparent objects	- Expensive and limited materials - Materials must be stored properly - Photopolymers release harmful gases
SLS	- Printing of complex and small shapes - Various high strength materials - No support structures - Customizable porosity - Studies shown to work with chemically active additives	- Expensive systems - Temperature instability may cause distortions

6 Materials and methods

This chapter will go over the preparation and synthesis of powdered Lithium Titanium Managese Oxide (LTMO) adsorbents, and their use in 3D-printing. In addition, the experimental setups for both powder and 3D-print sorption will be described.

6.1 Chemicals

The following chemicals were used in the synthesis of LTMOs: Titanium(IV) oxide (TiO2) (≥ 99%), Manganese(II) carbonate (MnCO3) (≥ 99.9%) from Sigma Aldrich, and Lithium carbonate (Li2CO3) (≥ 99.0%) from VWR Chemicals. Synthetic solutions used in sorption were created with Lithium sulfate monohydrate ($Li_2SO_4 \cdot H_2O$) (≥ 99%) from Thermo Scientific and Sodium sulfate anhydrous (Na_2SO_4) (≥ 99%) from J.T.Baker. HCl solutions for lithium elution were prepared from analytical grade 37 % HCl from Sigma Aldrich. Adjustment of pH was done with diluted solutions from 5 M Sodium hydroxide (NaOH) and 28% Ammonium hydroxide (NH_4OH) from Sigma Aldrich. All chemicals were of analytical grade. PA2200, a fine Polyamide 12 (PA12) powder from EOS GmbH was used as the structural material for the 3D-printed adsorbents.

6.2 Preparation of powder LTMO adsorbents

The LTMO adsorbents were prepared with differing molar ratios of Ti and Mn according to the following chemical formula: $Li_{1.33}(Ti_xMn_{1-x})_{1.67}O_4$, where x was varied. Three different samples were synthesized, one sample with x = 0.1 and another with x = 0.2 were prepared by the solid synthesis method, and a third sample of x = 0.2 by mixing an ethanol slurry. Each of the synthesized samples was split into three for calcination, resulting in 9 samples. The samples will be calcined at different temperatures to find out the combination of calcination temperature and x value with the best sorption performance.

The solid synthesis method is the simplest method for LIS synthesis and involves the mixing and crushing of powdered salts. Li_2CO_3, $MnCO_3$ and TiO_2 were weighed to achieve the molar ratio of Li, Mn and Ti for the chosen x value, and then mixed and ground thoroughly

using a mortar and pestle. The resulting powder mixture was dried in an oven overnight at 60 °C, and then split into three samples. One sample of LTMO was prepared by mixing the chemicals in 15 ml of pure ethanol over 60 minutes with a magnetic mixer. The resulting slurry was dried overnight at 100 °C, after which the dried mixture was ground into powder and split into three samples. The three split samples from each synthesized sample were calcined in a furnace at temperatures of 350 °C, 450 °C and 550 °C, with a heating rate of 5 °C/min. Summary of prepared LTMO samples is presented in Table 5.

Table 5. Summary of prepared LTMO samples.

X value	Preparation method	LTMO mass (g)	Li_2CO_3 mass (g)	$MnCO_3$ mass (g)	TiO_2 mass (g)	Total reagent mass (g)
0.2	Solid-state	10	3.02	9.45	1.64	14.11
0.2	Ethanol slurry	5	1.51	4.72	0.82	7.05
0.1	Solid-state	5	1.50	5.273	0.407	7.18

After calcination, the resulting 9 powder samples were all leached with a 0.5 M HCl solution for 48 hours in a shaker. The lithium in the LTMO is leached out and replaced with a hydrogen ion, forming HTMO samples ready for sorption. Samples were prepared for leaching by weighing 0.5 g of LTMO powder into a tube and adding 50 ml of 0.5 M HCl. After leaching, the samples were filtered to separate the HTMO from the acid, and then the samples were washed with deionized water until the filtrate reached a neutral pH. The washed HTMO samples were dried in an oven overnight at 60 °C.

6.3 Powder batch sorption experiments

The leached HTMO powder adsorbents were used in batch sorption experiments to determine their sorption and selectivity performance. Two solutions were prepared, one containing 100 mg/L of Li^+ to be used for sorption, and one containing 100 mg/L of Li^+ and 55 g/L of Na^+ to study selectivity. Experiments were conducted by adding 20 mg of each HTMO sample into 10 ml tubes with 10 ml of the prepared synthetic solution. Batch sorption studies were carried out over 24 hours by placing the samples on a shaker, after which, the solutions were filtered with a syringe filter and then prepared for analysis with AAS (Atomic Absorption Spectroscopy). All samples were analyzed with a Thermo Scientific iCE 3000

AAS instrument utilizing an acetylene-air flame and equipped with a deuterium lamp for background correction. All samples were diluted with 0.5 % HCl to fit within the range of the following series of standard solutions: 0.4 – 10 mg/L for lithium, 50 – 1500 mg/L for sodium, and 0.1 – 8 mg/L for manganese.

The effect of pH on sorption performance was studied with sorption experiments at pH values varying between 8 – 12. The pH of the synthetic adsorbate solutions was initially adjusted with NaOH, but this was changed to NH_4OH after the first sorption experiment in order to achieve more accurate analysis results for sodium. From the sorption results, the best performing X = 0.1 and X = 0.2 adsorbents were selected for use in 3D-printing. The effect of temperature on sorption performance was studied with powder sorption experiments.

6.4 Characterization of LTMO

X-ray diffraction (XRD) and Fourier-transform infrared spectroscopy (FTIR) were used for the characterization of the LTMO adsorbents. The LTMO adsorbents crystal structure was analyzed using a Bruker D8 powder XRD instrument with Cu Kα radiation at 40 kV and 40 mA. Scans were performed from 4 – 80° at 0.02°/2s with a step size of 0.02°.

The chemical composition of the LTMO adsorbents was analyzed with a Perkin Elmer Frontier FTIR system with attenuated total reflectance (ATR) sampling. Analysis was performed at the wavelength range of 4000 – 400 cm^{-1} with a resolution of 1 cm^{-1}.

The surface morphology of the LTMO adsorbents was studied using a Hitachi SU3500 scanning electron microscopy with energy dispersive spectroscopy (SEM-EDS) system. Scanning was performed with a 10 kV voltage, and images were taken at up to 320 times magnification.

6.5 Preparation of 3D-printed adsorbents

The 3D-printed adsorbents were manufactured using a Sharebot Snowwhite 2 SLS 3D printer outfitted with a reduced powder distributor. Three different adsorbent materials were used for 3D-printing: the optimal X = 0.1 and X = 0.2 adsorbents from powder batch

experiments, and a purchased LMO (X = 0) adsorbent. The adsorbent material cannot be printed by itself, so it must be mixed with a 3D-printable structural material, such as PA12. The adsorbents were mixed with PA12 at a mass ratio of 25% adsorbent and 75% PA12. For batch experiments, a lattice structure model was used for printing, and column experiments utilized a stackable disk model, both of which are shown in Figure 11.

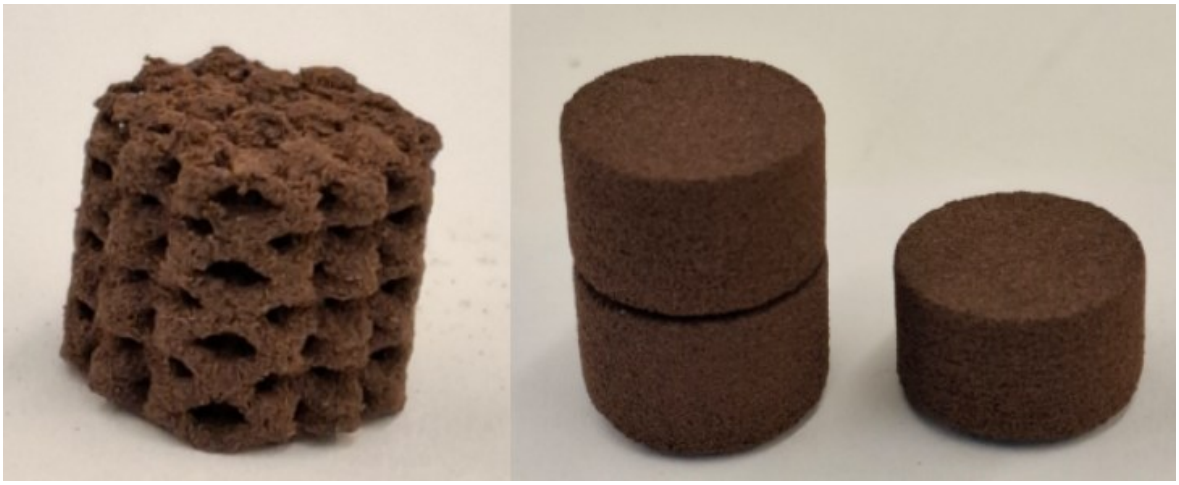

Figure 11. 3D-printed adsorbent shapes. Lattice (Left) and stackable disks (Right)

To ensure that printed objects are structurally robust, and that powder does not melt or cake in and around the objects, the printing parameters must be optimized for the used material mixture. As a baseline, the manufacturer recommended parameters for plain PA12 were used and then changed through trial and error. The prints utilized for column experiments require a lower laser power and laser power rate in order to create a porous structure within the printed object. After each print, the remaining powder in the printer was sieved and a small amount of previously unused powder mixture was mixed in prior to reusing the powder.

6.6 3D-print sorption experiments

For 3D printing, four different materials were chosen. Two best LTMO materials (x = 0.1, at 450 °C and x = 0.2 at 550 °C) were chosen based on results from powder sorption experiments. In addition, a purchased LMO (x = 0) was used as a reference material for comparison.

6.6.1 Batch

Batch experiments were performed by first eluting each of the 3D-printed lattice shapes in 50 ml of 0.5 M HCl over 48 hours. After elution, the prints were washed with deionized water and dried overnight. The sorption experiments were performed by adding a dried print into 10 ml of synthetic solution at pH values of 8, 10, and 12. After sorption, the solutions were analyzed to determine the sorption performance and manganese dissolution from prints during sorption. These results were used in selecting the optimal LTMO material for use in column experiments.

6.6.2 Column

Column experiments were performed with porous 3D-printed disks stacked in a glass column with an inner diameter of 15 mm and a heating jacket. The column was fed from the bottom, and the top was connected to an autosampler set to sample every 10 minutes. The parameters for the column experiment are shown in Table 6.

Table 6. Column experiment parameters.

Height	Volume	Material mass	Flow rate	Temperature	pH
14.0 cm	26.5 cm^3	15.0 g	1.00 ml/min	25.0 °C	12.0

The adsorbent material in the column was eluted with 0.5 M HCl and then washed with water. Initial elution was conducted by 2 hour elution followed by 1 hour of washing repeated 3 times. The first sorption-desorption cycle was performed with 14 hours of sorption and 14 hours of desorption. However, after receiving analysis data on when sorption and desorption was fully complete the following cycles were performed with 7 hour sorption followed by 4 hour desorption. The lithium and sodium containing solution was adjusted to pH 12, and the column was briefly rinsed with NH_4OH to increase the pH of the column, so that it does not negatively affect sorption performance. The column was used for 3 sorption-desorption cycles to measure the loss of performance between cycles, and a single sorption cycle was performed at a temperature of 55 °C utilizing a freshly printed column to compare performance at different temperatures.

7 Results and discussion

This chapter will discuss the results of the experimental part of the thesis, including characterization and sorption.

7.1 Materials characterization

The LTMO powder samples were characterized using XRD and FTIR to determine the presence of LTMO and the completeness of the calcination reaction at different temperatures.

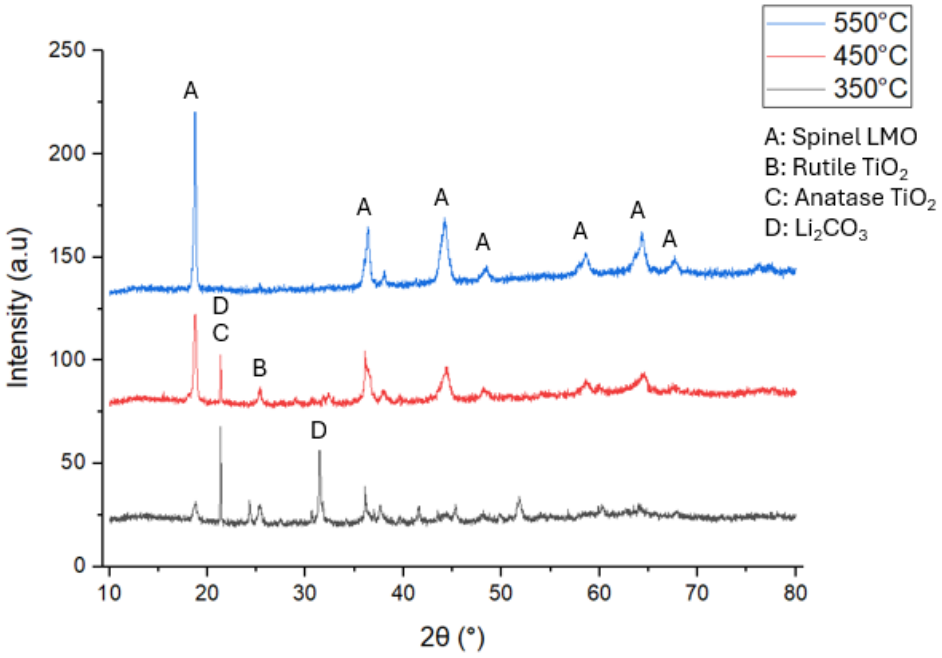

Figure 12. XRD patterns of LTMO powders with X = 0.2 ($Li_{1.33}(Ti_{0.2}Mn_{0.8})_{1.67}O_4$).

From the XRD patterns for LTMO X = 0.2 shown in Figure 12, peaks corresponding to spinel LMO (Ryu et al., 2019) can be seen at all calcination temperatures, however the peaks grow in intensity as temperature increases. At temperatures of 450 °C and 350 °C, peaks signifying the presence of rutile and anatase TiO_2 start appearing (Ryu et al., 2019), this could mean that parts of the TiO_2 did not react in these lower temperatures. At 550 °C, these peaks disappear, signifying that titanium reacted completely to form spinel LTMO. Peaks that could signify the presence of unreacted Li_2CO_3 (manganese-titanium) are also present

at temperatures of 450 °C and 350 °C. However, the peak at 21° could correspond to either Li_2CO_3 or anatase TiO_2.

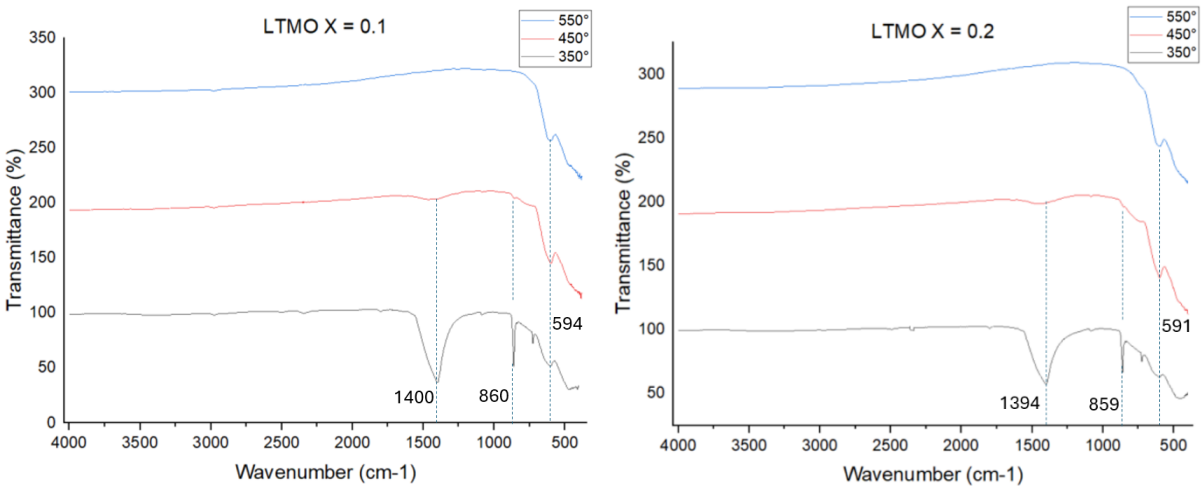

Figure 13. FTIR spectra of LTMO powders with X = 0.1 ($Li_{1.33}(Ti_{0.1}Mn_{0.9})_{1.67}O_4$) (left) and X = 0.2 ($Li_{1.33}(Ti_{0.2}Mn_{0.8})_{1.67}O_4$) (right).

As seen in Figure 13, the FTIR spectra for the LTMO powders at the same temperatures are similar to each other, while noticeable changes can be seen as temperature decreases. All samples present absorption bands at around 595 cm^{-1}, which signifies the presence of Mn-O bonds. Specifically, absorption bands in the range of 400 – 700 cm^{-1} indicate the vibrations of Mn(III)-O and Mn(IV)-O bonds (Song et al., 2024). Additional absorption bands are present in 350 °C samples at around 1400 cm^{-1} and 860 cm^{-1}. These absorption bands can also be seen in the 450 °C samples, but at a much lower intensity. Both of these bands align well with the spectrum of lithium carbonate (NIST, 2023), signifying the presence of unreacted lithium carbonate at lower temperatures.

The findings from the XRD patterns and FTIR spectra correlate well with each other. The presence of successfully synthesized material can be seen in both characterization methods, and the presence of lithium carbonate especially at 350 °C can be determined from both methods. Calcination at 350 °C is unviable due to the synthesis reaction not completing fully, which is signified by the presence of significant amounts of unreacted lithium carbonate. The presence of lithium carbonate is much smaller at 450 °C, and at 550 °C it is no longer present, signifying complete reaction.

The 3D-printed batch adsorbents were examined with SEM analysis to study the surface morphology of the material after 3D-printing.

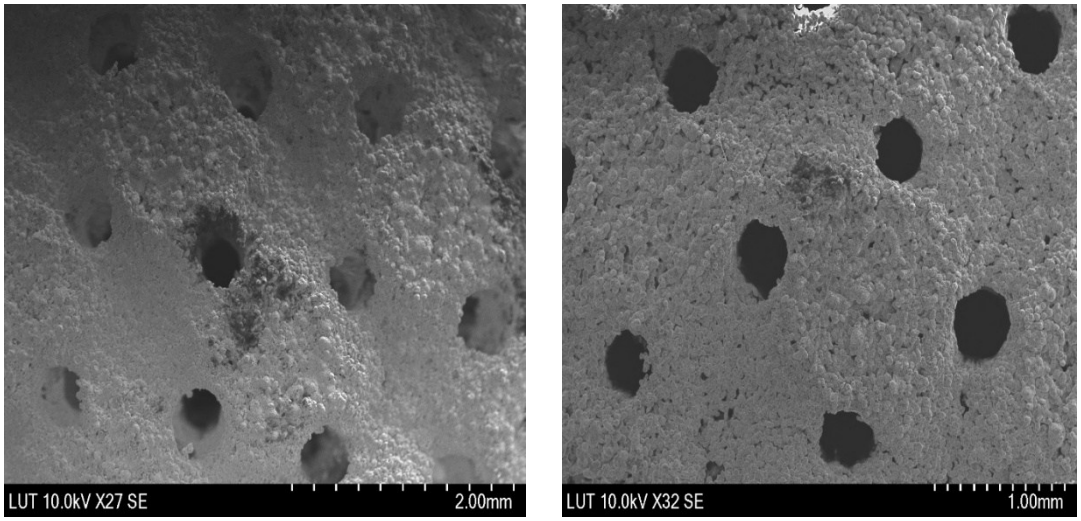

Figure 14. SEM image of 3D-printed batch adsorbent before (left) and after sorption (right), showing the holes inherent to the printed lattice structure.

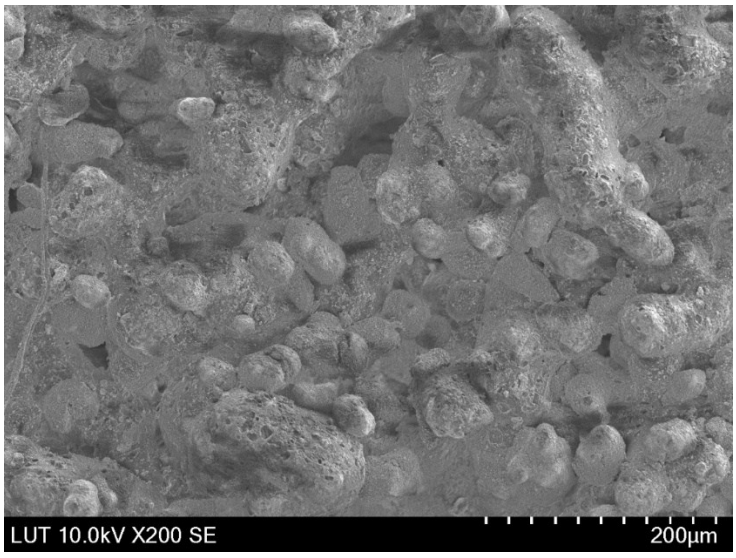

Figure 15. SEM image of 3D-printed batch adsorbent at 200-times magnification, highlighting the roughness of the 3D-printed surfaces.

As seen in Figure 14, the adsorbent does not show much difference in surface morphology before and after sorption. The SEM images show that the overall surface of the adsorbent is rough and consisting of granular spheres. In addition to the holes present in the 3D-print, the surface is also somewhat porous, with pores of various sizes seen throughout the surface, especially in the heavily magnified image shown in Figure 15.

7.2 Batch sorption with powders

Sorption experiments with powders were performed at room temperature with pH values between 8 – 12 by adjusting the pH of the synthetic solutions with NH_4OH.

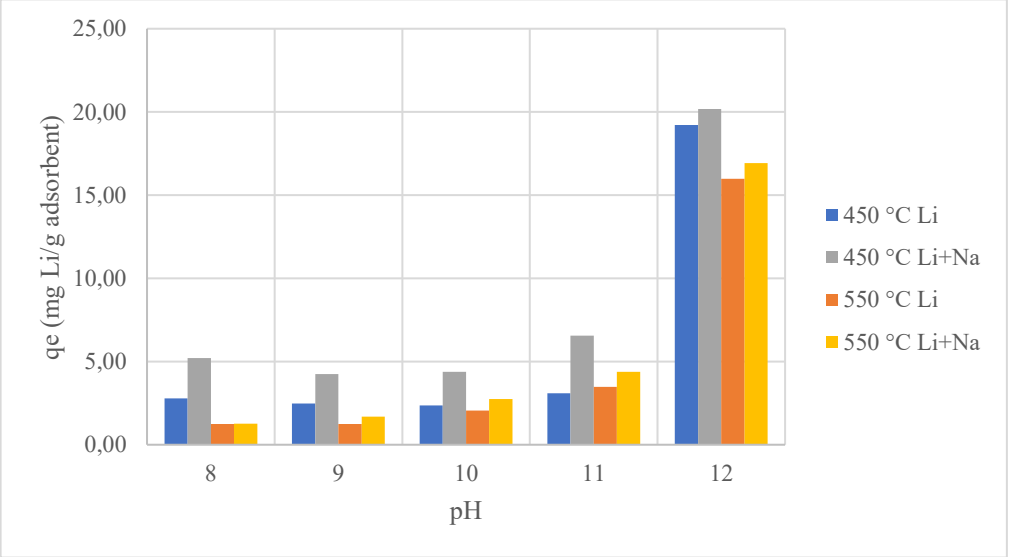

Figure 16. Sorption capacities of HTMO x = 0.1 powders at pH 8 – 12 in a lithium solution (100 mg/L) and in a mixed lithium + sodium solution (100 mg/L Li^+ + 55 g/L Na^+).

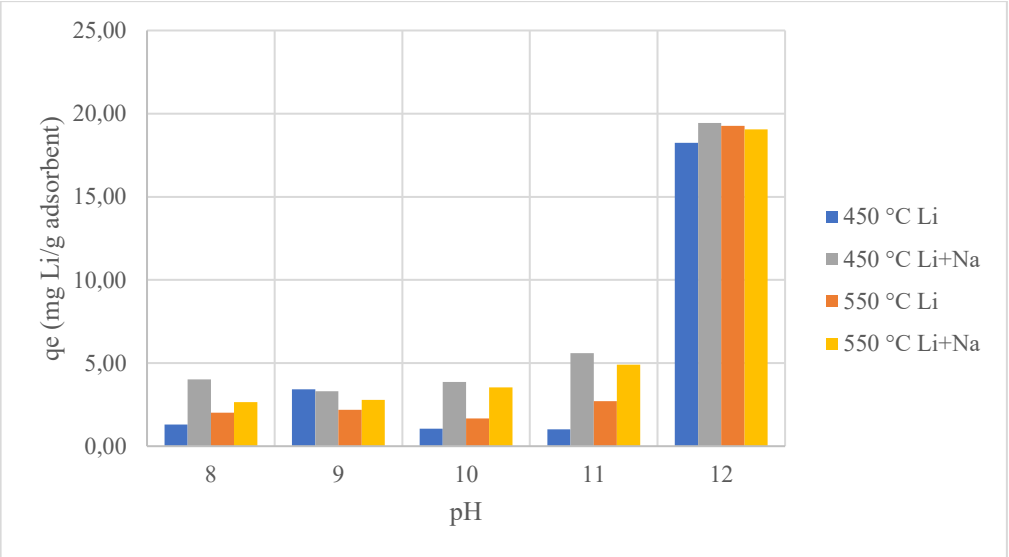

Figure 17. Sorption capacities of HTMO x = 0.2 powders at pH 8 – 12 in a lithium solution (100 mg/L) and in a mixed lithium + sodium solution (100 mg/L Li^+ + 55 g/L Na^+).

Figures 16 and 17 both show that the lithium sorption capacity generally increases with increasing pH levels. The change in capacity is modest at pH 8 – 10, where capacities largely

stay below 5 mg/g (0.72 mmol/g). A considerable increase in capacity can be seen at pH 11 with the 450 °C HTMO reaching capacities above 5 mg/g in the lithium and sodium containing solution. The sorption capacity heavily increases once pH 12 is reached, with capacities between 15 – 20 mg/g (2.16 – 2.88 mmol/g), which is three to four times larger than at pH 11. The effect of pH on the sorption performance of LISs is known in literature (Weng, D. et al., 2020). Increasing pH promotes the sorption of cations by providing more negatively charged surface sites on the adsorbent material for cations, such as Li^+, to adsorb onto (Speight, 2018). A higher pH value means that there are less H^+ ions present in the solution, resulting in less competition between H^+ and Li^+ for cavities within the ion-sieves crystal structure, and promoting the exchange of H^+ ions in the ion-sieve with the Li^+ ions in the solution.

At pH 12, the adsorbents have a removal-% of around 40 %, and in general, the sorption capacity of the powder adsorbents seems to increase in the solution containing 55 g/L of sodium in addition to 100 mg/L lithium, highlighting the high selectivity of the adsorbent. The 550 °C adsorbents show gradual improvements in capacity at pH 8 – 11, with the only exception being the X = 0.2 adsorbent at pH 10 in the lithium solution. On the other hand, the 450 °C adsorbent performance varies, with both increases and decreases in capacity as pH is increased. Nevertheless, the 450 °C adsorbents perform slightly better than the 550 °C adsorbents in the lithium and sodium containing solution, but the difference is very small, especially at pH 12 where the best overall performance is achieved.

The selectivity of the adsorbents for lithium in the sodium containing solution was studied by calculating the selectivity coefficients shown in table 7.

Table 7. Selectivity coefficients K for lithium in powder batch sorption.

pH	X = 0.1 450 °C	X = 0.1 550 °C	X = 0.2 450 °C	X = 0.2 550 °C
8	4.85	125	465	309
9	481	184	371	322
10	24.5	301	433	411
11	7.05	524	3.13	623
12	3560	2800	37.4	3330

Values of $K > 1$ indicate preference for lithium, while values of $K < 1$ indicate preference for sodium. In several cases, no reduction in sodium content was detected during analysis, resulting in very high coefficient values. The variance in the coefficient values is possibly caused by analytical error and interference caused by the AAS equipment.

In general, the behaviour of the X = 0.1 and X = 0.2 adsorbents is similar. Both show increases in capacity as pH is increased, with a large spike at pH 12. For both adsorbents, the capacity is also better in the sodium containing solution. All of the adsorbents show exceptional selectivity for lithium, even as sodium concentrations are 550 times higher than that of lithium. The best performing adsorbent is the X = 0.1 at 450 °C, and in the case of X = 0.2 adsorbents, the 450 °C performs only slightly better than the 550 °C adsorbent. From these results, X = 0.1 at 450 °C and X = 0.2 at 550 °C were chosen for use in 3D-printing experiments.

7.3 Sorption experiment with 3D-printed adsorbents

For utilization in 3D-printing, the chosen adsorbent materials, X = 0.1 at 450 °C, X = 0.2 at 550 °C, and the reference LMO, were mixed with PA12 as structural material at a mass ratio of 25 % adsorbent with 75 % PA12. Experiments were performed at pH 8 – 12 and at a temperature of 25 °C, apart from the effect of temperature studies.

7.3.1 Batch sorption

During the 3D-printing process the LMO adsorbent mixture resulted in successful prints with only relatively few adjustments in printer settings from the optimal PA12 printing settings. On the other hand, both LTMO adsorbents required different and extensive adjustments to result in printed adsorbents that could be used in batch sorption.

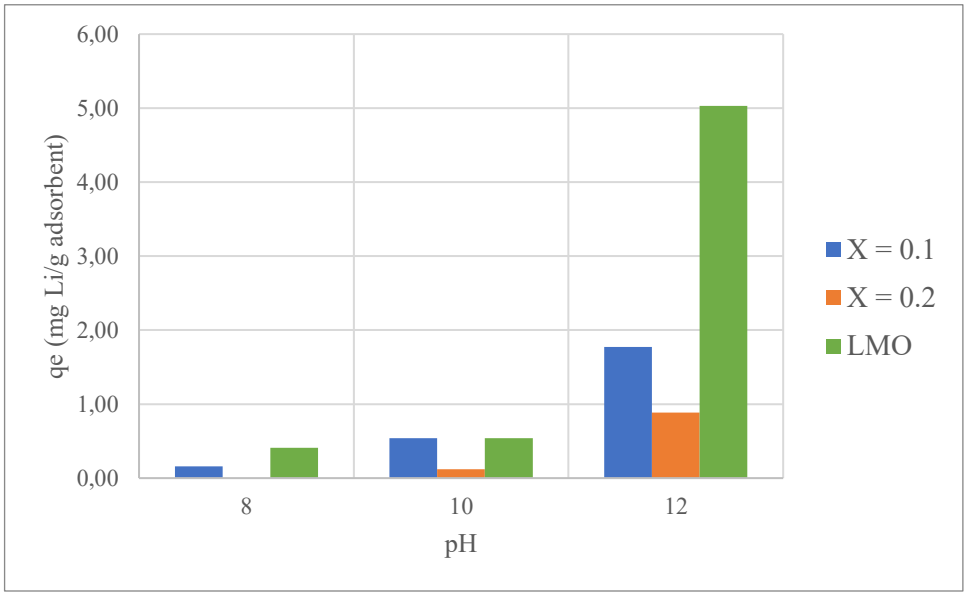

Figure 18. Sorption capacities of 3D-printed adsorbents in lithium containing solution (100 mg/L Li^+).

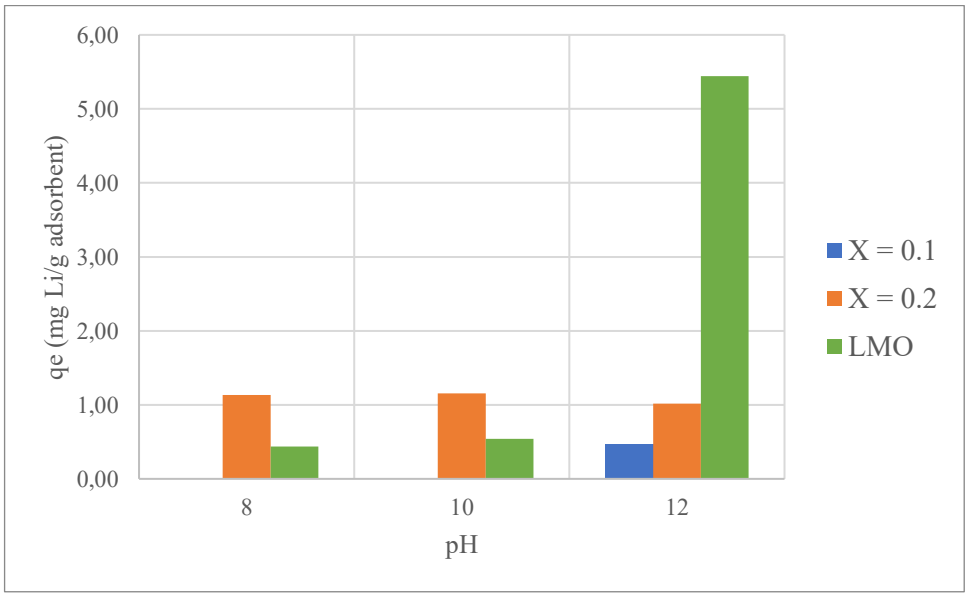

Figure 19. Sorption capacities of 3D-printed adsorbents in lithium and sodium containing solution (100 mg/L Li^+ + 55 g/L Na^+).

Figures 18 and 19 show that the sorption capacities of adsorbents are lower than that of powders, which is explained by the experiments being performed in the same amount of adsorbate solution and the much larger mass of the 3D-printed adsorbent in comparison to the powders. The LMO performs better than the LTMO adsorbents reaching removal-% of around 40 %, which is similar to values observed in the LTMO powders. The 3D-printed

LTMO however exhibits removal-% values of between 3 – 10 %, performing considerably worse than their powder counterparts. In terms of capacity, the X = 0.1 adsorbent performs much worse in the sodium containing solution than in the lithium only solution, and conversely, the X = 0.2 performs better in the sodium containing solution. The difference in capacities between LTMO powders and 3D-prints results from the ratio of LTMO to PA12 during the 3D-printing process, and the capacity of the prints will most certainly increase with an increasing amount of active material. This could be caused by either the 3D-printer itself or the material. Another possible but unstudied cause is the changing of the printing settings affecting printing conditions, as the LMO performs well with only small adjustments to printer chamber temperature, while the LTMO required a combination of several changes in temperatures, laser power, layer height and waiting times.

Table 9. Selectivity coefficients K for lithium in 3D batch sorption.

pH	X = 0.1 450 °C	X = 0.2 550 °C	LMO
8	-0.53	18.2	0.631
10	-2.27	5.13	197
12	158	1.61	40.9

Table 9 shows that the selectivity of the 3D-printed adsorbents is very good similarly to the powder adsorbents. Notable exceptions in these results are the X = 0.2 LTMO at pH 12 and the LMO at pH 8. While the X = 0.2 still shows preference for lithium, the LMO at pH 8 shows preference for sodium. These two results could be considered as outliers caused by large variations in analysis results for sodium caused by the inherent interference in AAS equipment. In addition, analyses for the X = 0.1 sorbent at pH 8 and 10 did not show a change in lithium content and no sorption occurred.

7.3.2 Effect of temperature in batch sorption

To study the effect of temperature on sorption performance, experiments were performed with the X = 0.2 LTMO at temperatures of 35 °C, 45 °C, and 55 °C, while keeping pH at 12 to ensure best sorption performance.

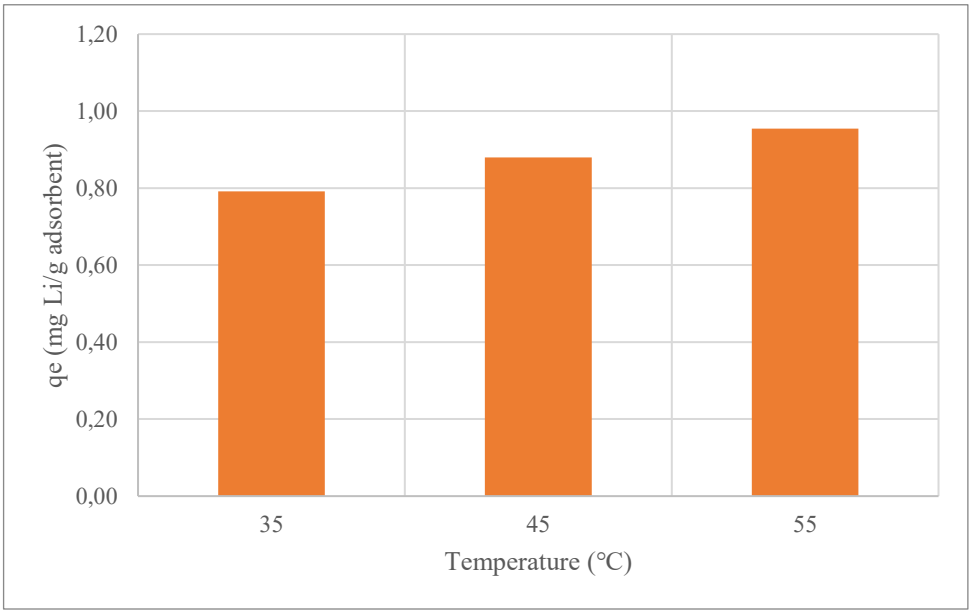

Figure 20. Effect of temperature on sorption capacity for powder LTMO (X = 0.2 at 550 °C) adsorbent in lithium and sodium containing solution (100 mg/L Li^+ + 55 g/L Na^+).

Figure 20 shows that the adsorbent exhibits steadily increasing sorption performance as temperature is increased. The increase in capacity is 11.1 % from 35 °C to 45 °C, and 8.5 % from 45 °C to 55 °C.

7.3.3 Chemical stability

The main problem of LMO adsorbents is the amount of manganese dissolved during sorption, negatively affecting the cyclical performance of the adsorbent while also releasing pollutants into the adsorbate solution. To prevent manganese dissolution, LMOs are doped with other metals to increase structural stability. The combination of manganese and titanium into LTMO sieves has been shown to provide good performance while also lowering the dissolution of manganese (Ryu et al., 2019). The amount of dissolved manganese was analyzed from the adsorbate solution of the 3D-printed batch adsorbents at pH 8 – 12 after sorption was finished.

Table 10. Amount of manganese dissolved from 3D-printed adsorbents after sorption.

pH	X = 0.1 450 °C	X = 0.2 550 °C	LMO
8	43.69 %	68.26 %	0.59 %
10	4.00 %	0.48 %	0.25 %
12	0.79 %	0.24 %	0.84 %

As shown in table 10, The LMO exhibits relatively low amounts of dissolved manganese but rises to 0.84 % of total manganese dissolved at pH 12. The LTMO adsorbents experience drastic amounts of dissolution at pH 8, rendering them practically useless after just one sorption cycle. However, as pH increases, the amount of dissolved manganese decreases rapidly, reaching lower levels than the LMO at pH 12. The X = 0.2 at 550 °C adsorbent experiences less manganese dissolution than both the LMO and X = 0.1 at 450 °C adsorbents, while the least amount of dissolution also coincides with the best sorption performance at pH 12. While the difference in dissolution is fairly small over one sorption cycle, the difference in total dissolution may be slightly significant over multiple cycles. The LTMO X = 0.2 at 550 °C shows clear advantages over the X = 0.1 at 450 °C in both sorption and resistance to manganese dissolution. This can be explained by the findings during characterization, where the synthesis reaction was shown to be only partially complete at 450 °C, while all the reagents had reacted to form the LTMO at 550 °C. A fully complete synthesis reaction may enhance the phase formation of the LTMO, and therefore increase its resistance to manganese dissolution.

7.3.4 Column sorption

For column sorption, the X = 0.2 at 550 °C adsorbent was chosen over the X = 0.1 at 450 °C due to its good performance, lower manganese dissolution, and higher maximum sorption capacity as studied in previous experiments. In the column experiments, the performance of the adsorbent material is sought to be improved over the batch experiments, and the cyclical performance of the material is studied to see the potential of reusing the adsorbent. The reusability of the adsorbent material is important to ensure that the lithium recovery process

is economically feasible and that it does not produce too much unnecessary waste, such as dissolved manganese or spent and unusable adsorbents. The sorption performance of the X = 0.2 at 550 °C material over three sorption-desorption cycles is shown in Figure 21 as breakthrough curves.

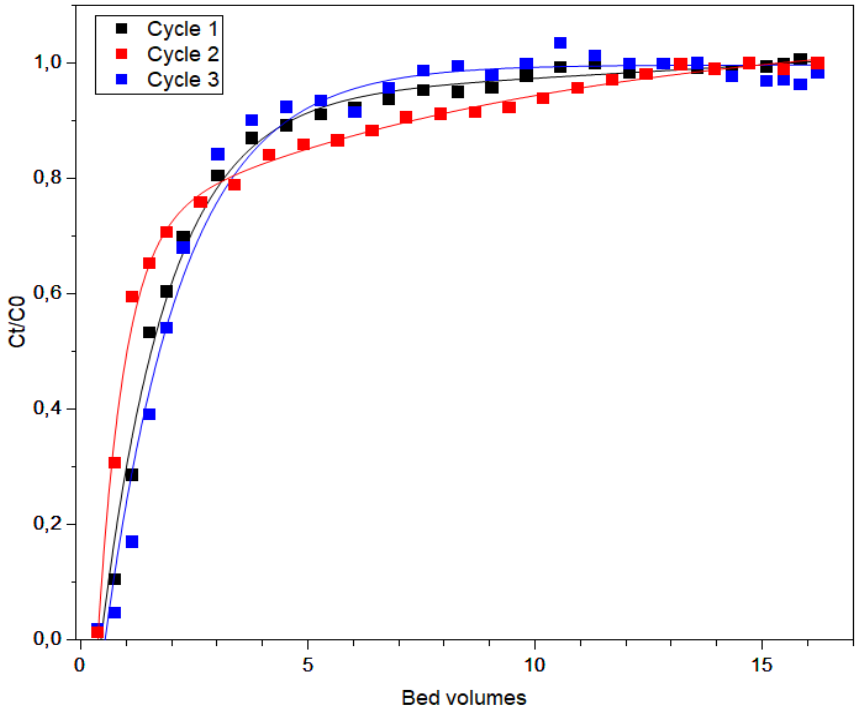

Figure 21. Breakthrough curves for three sorption cycles for X = 0.2 at 550 °C column.

While the sorption process for the column can take up to 6 hours to reach maximum capacity, the desorption of lithium is a much faster process, with the majority of lithium being desorbed within the first hour of the desorption cycle. During sorption, maximum capacity was reached after around 13.2 bed volumes (350 minutes) for cycle 1, 11.3 bed volumes (300 minutes) for cycle 2, and 8.3 bed volumes (220 minutes) for cycle 3, signifying a decrease in sorption performance over each cycle.

Table 11. Sorption capacities of column over 3 sorption-desorption cycles.

Cycle	q_e (mg/g)	q_e (mmol/g)	% decrease
1	1.68	0.242	
2	1.59	0.230	5.006 %
3	1.54	0.223	3.092 %

The adsorbent material experiences performance loss over sorption cycles due to the dissolution of manganese from both highly alkaline conditions during sorption, and acidic conditions during desorption. The adsorbent exhibits improved performance when applied in a column compared to batch sorption. Table 11 shows that the sorption capacity decreases by 5 % after the first cycle, and 3 % after the second cycle, signifying that the majority of performance loss may happen during the first few cycles, and the cyclical performance may stabilize later on.

7.3.5 Effect of temperature in column sorption

The positive effect of increasing temperature on sorption capacity was shown during the batch sorption experiments. A freshly printed column was used for sorption at an increased temperature to examine the effect of temperature in the column setup. The breakthrough curves for the temperature experiments are shown in Figure 22.

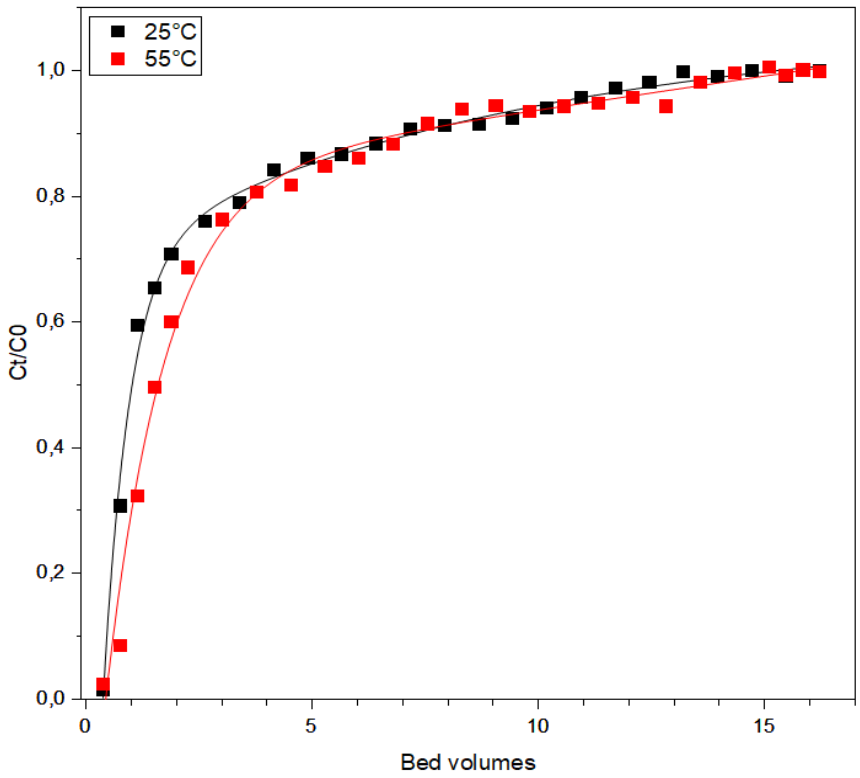

Figure 22. Breakthrough curve for sorption at 25 °C for X = 0.2 at 550 °C column.

Table 12. Sorption capacities at different temperatures in column application.

Temperature (°C)	q_e (mg/g)	q_e (mmol/g)	% increase
25	1.68	0.241	
55	2.01	0.289	19.7 %

Table 12 shows the change in sorption capacity with increasing temperature. The same effect can be seen for the column as for the batch adsorbents, however, the increase in performance for the column is impressive at almost 20 % from 25 °C to 55 °C. Temperature typically increases mass transfer and therefore sorption performance, solidifying it as an important parameter to consider during sorption, alongside pH levels.

7.4 Sorption performance of similar ion-sieves

The 3D-printed LTMO batch and column adsorbents are compared with other 3D-printed LIS adsorbents found in literature in table 13.

Table 13. Comparison of 3D-printed LIS adsorbents from other studies (pH = 12, T = 25°C).

Adsorbent	Ion sieve type	Active material content (w%)	Solution Li^+ concentration (mg/L)	Sorption capacity (mg/g)	Reference
3D LTMO (Batch)	Titanium-manganese	25	100	1.02	This thesis
3D LTMO (Column)	Titanium-manganese	25	100	1.68	This thesis
3D-LIS-H	Titanium	75	200	12.3	(Yu et al., 2023)
3D-PA@HTO	Titanium	10	20	1.5	(Bandina et al., 2025)
3D LMO	Manganese	66	50	5.4	(Martínez et al., 2024)

The capacity of the LTMO adsorbents is on the lower end of the compared materials. This can be at least partially explained by the differences in active material contents between the

adsorbents. While the lowest active material content is at 10 %, the LTMO is still among the lower end at 25 %, while the rest have high contents of 66 % and 77 %. Another factor is the choice of ion sieve material, the LMO adsorbent by Martínez et al. (2024) performs better than the LTMO adsorbent when only sorption capacity is considered, correlating with findings in this thesis. While the capacity of the LTMO is lower, the increased resistance to manganese dissolution is significant, and the performance of the adsorbent could be improved by increasing the active material content.

Table 14. Comparison of the synthesized powder LTMO adsorbent with LTMO from other studies.

X value	Calcination temperature (°C)	Solution Li^+ concentration (mg/L)	Sorption temperature	Sorption capacity (mg/g)	Reference
0.2	550	100	25	19.27	This thesis
0.5	600	100	45	32.32	(Ding et al., 2023)
0.1	500	60	25	~17	(Ryu et al., 2019)

Only a few studies have been conducted on LTMO adsorbents specifically, and those studies focus on their utilization as powders. While the focus of this thesis is on 3D-printed materials, the synthesized LTMO powder can be compared to powders from other studies, which are shown in table 14. In the study by Ding et al. (2023), a much higher sorption capacity is achieved in optimal conditions. The difference compared to the LTMO synthesized in this thesis can be explained by the difference in sorption temperature and the choice of acid used during elution. The highest capacity of 32.32 mg/g was achieved using DL-malic acid, while experiments were also conducted with citric acid for a capacity of 25.67 mg/g, and tartaric acid for 25.99 mg/g. The chosen acid has a clear effect on sorption capacity, caused by complexation of lithium especially in the case of organic acids (Li, L. et al., 2024), providing another factor to consider for future studies with 3D-printed LTMOs.

Ryu et al. (2019) found that within the range of 500 – 700 °C calcination temperature and X values of 0.1, 0.3, and 0.5, the optimal material was a X = 0.1 LTMO calcined at 500 °C. The experiments in this thesis show that at calcination temperatures of 450 °C and below,

the synthesis reaction is incomplete, potentially contributing to decreased sorption performance and dissolution resistance at least for 3D-printed adsorbents.

7.5 Challenges of ion-sieve sorbents

The main challenges of utilizing ion-sieves are improving their sorption capacity and chemical stability against dissolution. Dissolution can severely reduce the performance of the sorbent over several sorption-desorption cycles, while also introducing pollutants into the adsorbate (Chen et al., 2024). Manganese-based ion-sieves are particularly prone to dissolution, as Mn^{3+} present in the structure converts into more soluble Mn^{2+} during sorption, but titanium-based ion-sieves also experience some dissolution losses in the form of soluble Ti^{4+} (Chen et al., 2024; Weng, D. et al., 2020).

The way these challenges are being addressed in research is by doping, with the aim of replacing ions prone to dissolution with other metal ions (Chen et al., 2024; Weng, D. et al., 2020). Doping with monovalent ions such as Na^{+} and K^{+} result in substituting Li^{+} ions within the ion-sieve structure and have been shown to result in similar capacities as unmodified sieves, while providing slightly improved chemical stability (Chen et al., 2024). Monovalent ions are effective for doping manganese-based sieves, as they replace Mn^{3+} ions within the structure (Chen et al., 2024; Weng, D. et al., 2020). The effect of doping varies depending on the dopant used, with Mg^{2+} providing slightly improved capacity and stability, Fe^{3+} resulting in slightly lower capacity with considerably improved stability, and Al^{3+} providing improved capacity with good stability (Chen et al., 2024).

The method of applying ion-sieves in an industrial setting is a challenge, as a powdered sorbent may not always be suitable. However, 3D-printing shows promise as a solution. Monolithic 3D-printed ion-sieve sorbents have been shown to retain good sorption capacities while also having improved mechanical strength, making them suitable for industrial use in lithium recovery from brines (Yu et al., 2023). 3D-printing allows for the production of adsorbents of various shapes and sizes, while providing a porous structure which allows for high flow rates while also improving mass transfer (Lahtinen, 2019).

8 Conclusions

The goal of this thesis was the synthesis and development of highly selective and 3D-printable adsorbent materials, known as ion sieves, to recover lithium from battery recycling raffinates. In the literature review, the production, use cases, and recycling of lithium were reviewed. The increasing demand for batteries is one of the driving forces behind increasing lithium demand, which results in an increasing number of end-of-life batteries fit for recycling. Typical battery recycling processes utilize a combination of pyro- and hydrometallurgical methods, but the recovery of lithium is often incomplete. Ion sieves are a promising option for lithium recovery from spent battery raffinates, as they have a good capacity for sorption while being extremely selective due to a crystal structure which limits the sorption of metal ions larger than lithium. The use of chemically active additives in 3D-printing to print adsorbent modules has been studied previously, with SLS 3D-printing being feasible for creating porous adsorbents that allow for high flow rates while increasing contact with the active material and facilitating improved mass transfer.

While previous studies have focused mostly on manganese or lithium-based ion sieves and doping them with various metals to increase performance and stability, very few studies exist on combining the high performance of manganese with the stability of titanium into lithium titanium-manganese oxides, or LTMOs. The synthesis of LTMO powders was conducted at different synthesis conditions to achieve optimal performance, and the materials were characterized with FTIR and XRD to study the completeness of the synthesis.

Batch sorption experiments on synthesized powders revealed that the adsorbent performs exceedingly well at pH 12, while lower values result in drastically reduced performance. In general, the adsorbent performed better in a synthetic battery raffinate solution containing large amounts of sodium, compared to a plain lithium solution. Adsorbents with a ratio of 10 % titanium to manganese performed better when synthesized at 450 °C, while a titanium ratio of 20 % showed better performance with a synthesis temperature of 550 °C.

The LTMO adsorbent was prepared for 3D-printing by mixing it with PA12 as a structural material. Adsorbents were printed as lattice shapes to be used in batch sorption, and as stackable porous disks to be used in column sorption. While the printed batch adsorbents did not show performance on the level of powder adsorbents, the effectiveness of the adsorbent

in column experiments was good. Experiments with 3D-printed adsorbents showed that in addition to high pH values, the performance of the adsorbent improves with increasing temperature. While the performance increase was minor in batch sorption, column sorption resulted in a roughly 20 % increase in performance when temperature was increased from 25 °C to 55 °C. The amount of manganese dissolved from printed adsorbents was very low for the synthesized LTMO adsorbent at 0.24 % over one cycle, while a manganese-based LMO adsorbent used as comparison experienced 0.84 % manganese dissolution. The difference confirms that the mixing of manganese and titanium results in a more stable adsorbent structure, that is more resistant to dissolution.

Experiments on adsorbent selectivity showed that the LTMO adsorbent is extremely selective for lithium, even in the presence of much larger amounts of sodium. In a solution containing 100 mg/L of lithium alongside 55 g/L of sodium, no sodium was adsorbed in the majority of cases.

In conclusion, the LTMO adsorbent fulfils its purpose as a highly selective adsorbent for lithium. Further studies could be conducted on how they are utilized in sorption and seeking more optimized sorption conditions. In this thesis, the 3D-printed adsorbents utilized for batch sorption closely resemble packing materials used in packed columns in both shape and size, so their potential as a column packing material could be studied. In addition, 3D-printing allows for the creation of objects of numerous different shapes and sizes, resulting in potentially more optimal adsorbent shapes or ways to use them. A very important area of study is the conditions and cyclical performance of the adsorbents. This thesis explored sorption temperatures of up to 55 °C with great results, but the printed adsorbent structure can certainly withstand higher temperatures, as it is synthesized at up to 550 °C and 3D-printed at between 150 – 160 °C. The choice of acid used in elution is important for the cyclical performance, manganese dissolution, and desorption speed of the adsorbent. While this thesis only used HCl, it is important to study how other acids perform, with special interest being placed on H_2SO_4 due to its high cost effectiveness in industry.

References

Arote, S. A. (2022). *Lithium-Ion and Lithium-Sulfur Batteries : Fundamentals to Performance*. IOP Publishing. 10.1088/978-0-7503-4881-2

Awad, A., Fina, F., Goyanes, A., Gaisford, S., & Basit, A. W. (2020). 3D printing: Principles and pharmaceutical applications of selective laser sintering. *International Journal of Pharmaceutics, 586*, 119594. 10.1016/j.ijpharm.2020.119594

Bae, H., & Kim, Y. (2021). Technologies of lithium recycling from waste lithium ion batteries: a review. *Materials Advances, 2*(1), 3234–325. 10.1039/d1ma00216c

Bandina, E., Elkabous, M., Iurchenkova, A., Ouardi, Y. E., & Repo, E. (2025). 3D-printed polyamide-H2TiO3 composite for selective lithium adsorption: Insights from experimental and theoretical dynamic simulations studies. *Minerals Engineering, 231*, 109470. 10.1016/j.mineng.2025.109470

Bártolo, P. J. (2011). *Stereolithography Materials, Processes and Applications*. Springer US. 10.1007/978-0-387-92904-0

Baum, Z. J., Bird, R. E., Yu, X., & Ma, J. (2022). Lithium-Ion Battery Recycling─Overview of Techniques and Trends. ACS Energy Letters, 7(2), 712–719. 10.1021/acsenergylett.1c02602

Byrappa, K., & Yoshimura, M. (2013). *Handbook of Hydrothermal Technology (2nd Edition)* (2nd ed.). Elsevier. 10.1016/C2009-0-20354-0

Chen, Q., Chen, Z., Li, H., & Ni, B. (2024). Advanced lithium ion-sieves for sustainable lithium recovery from brines. *Sustainable Horizons, 9*, 100093. 10.1016/j.horiz.2024.100093

Colledani, M., Gentilini, L., Mossali, E., & Picone, N. (2023). A novel mechanical pre-treatment process-chain for the recycling of Li-Ion batteries. *CIRP Annals, 72*(1), 17–20. 10.1016/j.cirp.2023.04.068

Dabrowski, A. (2001). Adsorption — from theory to practice. *Advances in Colloid and Interface Science, 93*(1), 135–224. 10.1016/S0001-8686(00)00082-8

Davim, J. P., & Dave, H. K. (2021). *Fused deposition modeling based 3D printing*. Springer.

Determining the Price of Minerals: A Transfer Pricing Framework for Lithium (2024). OECD Publishing. 10.1787/a607ff0a-en

Ding, Y., Nhung, N. T. H., An, J., Chen, H., Liao, L., He, C., Wang, X., & Fujita, T. (2023). Manganese-Titanium Mixed Ion Sieves for the Selective Adsorption of Lithium Ions from an Artificial Salt Lake Brine. *Materials, 16*(11), 4190. 10.3390/ma16114190

Dong, C., Liu, C., Qin, Z., Deng, J., & Zhu, Y. (2025). A comprehensive overview of decommissioned lithium-ion battery recycling: Towards green and economical. *Separation and Purification Technology, 354*, 128929. 10.1016/j.seppur.2024.128929

Gebhardt, A., Kessler, J., & Thurn, L. (2019). *3D printing understanding additive manufacturing* (2nd ed.). Hanser.

Godec, D., Gonzalez-Gutierrez, J., Nordin, A., Pei, E., & Ureña Alcázar, J. (2022). *A Guide to Additive Manufacturing* (1st ed.). Springer International Publishing. 10.1007/978-3-031-05863-9

Gratz, E., Qina, S. A., Apelian, D., & Wang, Y. (2014). A closed loop process for recycling spent lithium ion batteries. *Journal of Power Sources, 262*, 255–262. 10.1016/j.jpowsour.2014.03.126

He, L., Sun, S., & Yu, J. (2018). Performance of LiNi1/3Co1/3Mn1/3O2 prepared from spent lithium-ion batteries by a carbonate co-precipitation method. *Ceramics International, 44*(1), 351–357. 10.1016/j.ceramint.2017.09.180

Hettesheimer, T., Hirzel, S., & Roß, H. B. (2018). Energy savings through additive manufacturing: an analysis of selective laser sintering for automotive and aircraft components. *Energy Efficiency, 11*(5), 1227–1245. 10.1007/s12053-018-9620-1

Huang, B., Pan, Z., Su, X., & An, L. (2018). Recycling of lithium-ion batteries: Recent advances and perspectives. Journal of Power Sources, 399, 274–286. 10.1016/j.jpowsour.2018.07.116

IEA. (2024). *Global Critical Minerals Outlook.* Washington: International Energy Agency.

Kaczorowska, M. A. (2024). Novel and Sustainable Materials for the Separation of Lithium, Rubidium, and Cesium Ions from Aqueous Solutions in Adsorption Processes-A Review. *Materials, 17*(24), 6158. 10.3390/ma17246158

Kang, J., Sohn, J., Chang, H., Senanayake, G., & Shin, S. M. (2010). Preparation of cobalt oxide from concentrated cathode material of spent lithium ion batteries by hydrometallurgical method. *Advanced Powder Technology : The International Journal of the Society of Powder Technology, Japan, 21*(2), 175–179. 10.1016/j.apt.2009.10.015

Kruth, J., Mercelis, P., Vaerenbergh, J., Froyen, L., & Rombouts, M. (2005). Binding Mechanisms in Selective Laser Sintering and Selective Laser Melting. *Rapid Prototyping Journal, 11*, 26–36. 10.1108/13552540510573365

Kumar, S. (2020). *Additive Manufacturing Processes* (1st ed.). Springer International Publishing. 10.1007/978-3-030-45089-2

Łacinnik, K., Szymon, W., Mikołajczak Wojciech, Artur, M., & Wojciech, S. (2025). Electrowinning of Nickel from Lithium-Ion Batteries. Materials, 18(24), 5653. 10.3390/ma18245653

Lahtinen, E. (2019). *Chemically Functional 3D Printing : Selective Laser Sintering of Customizable Metal Scavengers*

Li, J., Zhang, L., Wang, H., & Cui, Q. (2025). Synergistic regulation mechanism of Co/CTAB in titanium-based ion sieves and its adsorption extraction lithium performance from post-Li2CO3 precipitation liquor. Separation and Purification Technology, 376, 133838. 10.1016/j.seppur.2025.133838

Li, L., Li, Y., & Zhang, G. (2024). Summary of Pretreatment of Waste Lithium-Ion Batteries and Recycling of Valuable Metal Materials: A Review. *Separations, 11*(7), 196. 10.3390/separations11070196

Li, X., Chen, L., Chao, Y., Chen, W., Luo, J., Xiong, J., Zhu, F., Chu, X., Li, H., & Zhu, W. (2020). Amorphous TiO2-Derived Large-Capacity Lithium Ion Sieve for Lithium Recovery. *Chemical Engineering & Technology, 43*(9), 1784–1791. 10.1002/ceat.201900374

Li, X., Li, X., Chen, G., Li, H., Duan, Y., Sun, Y., Tiraferri, A., & Liu, B. (2025). Efficient recovery of lithium from spent lithium-ion battery raffinate by Mn and Al-based adsorbents: pretreatment, adsorption mechanism, and performance comparison. *Separation and Purification Technology, 354*, 128652. 10.1016/j.seppur.2024.128652

Li, Y., Yang, Z., & Ma, P. (2023). Research Progress on New Types of H2TiO3 Lithium-Ion Sieves: A Review. Metals (Basel), 13(5), 977. 10.3390/met13050977

Marcinov, V., Klimko, J., Takáčová, Z., Pirošková, J., Miškufová, A., Sommerfeld, M., Dertmann, C., Friedrich, B., & Oráč, D. (2023). Lithium Production and Recovery Methods: Overview of Lithium Losses. *Metals, 13*(7)10.3390/met13071213

Marthi, R., Asgar, H., Gadikota, G., & Smith, Y. R. (2021). On the Structure and Lithium Adsorption Mechanism of Layered H2TiO3. *ACS Applied Materials & Interfaces, 13*(7), 8361–8369. 10.1021/acsami.0c20691

Martínez, O.,Jair Licea, Delgado, B. G. S., Rodríguez, L. M. G., Sequeda, J. F. R., Rivera, G. L. D., Martínez, R. B., & De Haro Del Río, D. A. (2024a). Fabricating Ion Sieves by 3D Printing for Selective Lithium Adsorption from Brines. *ChemistrySelect (Weinheim), 9*(27), n/a. 10.1002/slct.202401347

Meng, F., McNeice, J., Zadeh, S. S., & Ghahreman, A. (2021). Review of Lithium Production and Recovery from Minerals, Brines, and Lithium-Ion Batteries. *Mineral Processing and Extractive Metallurgy Review, 42*(2), 123–141. 10.1080/08827508.2019.1668387

Meshram, P., Abhilash, Pandey, B. D., Mankhand, T. R., & Deveci, H. (2016). Comparision of Different Reductants in Leaching of Spent Lithium Ion Batteries. *Jom (1989), 68*(10), 2613–2623. 10.1007/s11837-016-2032-9

Meshram, P., Pandey, B. D., & Mankhand, T. R. (2015). Hydrometallurgical processing of spent lithium ion batteries (LIBs) in the presence of a reducing agent with emphasis on

kinetics of leaching. *Chemical Engineering Journal (Lausanne, Switzerland : 1996), 281*, 418–427. 10.1016/j.cej.2015.06.071

Natarajan, J., Cheepu, M., & Yang, C. (2021). *Advances in Additive Manufacturing Processes*. Bentham Science Publishers.

Neumann, J., Petranikova, M., Meeus, M., Gamarra, J. D., Younesi, R., Winter, M., & Nowak, S. (2022). Recycling of Lithium-Ion Batteries—Current State of the Art, Circular Economy, and Next Generation Recycling. *Advanced Energy Materials, 12*(17), n/a. 10.1002/aenm.202102917

NIST. (2023). *Lithium Carbonate.* U.S. National Institute of Standards and Technology. https://webbook.nist.gov/cgi/cbook.cgi?ID=B6000502&Mask=80

Ranjbar, M., Ehteshamzadeh, M., & Zandvakili, S. (2014). Synthesis of a nanostructure ion sieve with improved lithium adsorption capacity. *Micro & Nano Letters, 9*, 455–459. 10.1049/mnl.2014.0086

Ruthven, D. M. (1984). *Principles of adsorption and adsorption processes*. Wiley.

Ryu, T., Shin, J., Ghoreishian, S. M., Chung, K., & Huh, Y. S. (2019). Recovery of lithium in seawater using a titanium intercalated lithium manganese oxide composite. *Hydrometallurgy, 184*, 22–28. 10.1016/j.hydromet.2018.12.012

Sandhya, C. P., John, B., & Gouri, C. (2016). Synthesis, characterization and electrochemical evaluation of mixed oxides of nickel and cobalt from spent lithium-ion cells. *RSC Advances, 6*(115), 114192–114197. 10.1039/C6RA22439C

Shuva, M., & ASW, K. (2013). Hydrometallurgical Recovery of Value Metals from Spent Lithium Ion Batteries. *American Journal of Materials Engineering and Technology, 1*, 8–12. 10.12691/materials-1-1-2

Sicius, H. (2024). *Handbook of the Chemical Elements* (1st ed.). Springer Berlin Heidelberg. 10.1007/978-3-662-68921-9

Song, L., Liu, M., Nian, M., & Yang, G. (2024). Preparation of HMn2O4 lithium-ion sieves with low manganese dissolution loss for improved cycling stability. *RSC Advances, 14*(28), 19795–19805. 10.1039/D4RA02757D

Speight, J. G. (2018). *Reaction mechanisms in environmental engineering : analysis and prediction*. Butterworth-Heinemann, an imprint of Elsevier.

Sun, X., Radovanovic, P. V., & Cui, B. (2015). Advances in spinel Li4Ti5O12 anode materials for lithium-ion batteries.*39*(1), 38–63. 10.1039/c4nj01390e

Tabares, F. L. (2013). *Lithium : technology, performance and safety*. Nova Science Publishers, Inc.

Tangkas, I. W., Sujoto, V. S. H., Astuti, W., Jenie, S. N. A., Anggara, F., Utama, A. P., Petrus, H. T. B. M., & Sutijan. (2023). Synthesis of Titanium Ion Sieves and Its Application for Lithium Recovery from Artificial Indonesian Geothermal Brine. *Journal of Sustainable Metallurgy, 9*(2), 613–624. 10.1007/s40831-023-00664-7

Thompson, D. L., Hartley, J. M., Lambert, S. M., Shiref, M., Harper, G. D. J., Kendrick, E., Anderson, P., Ryder, K. S., Gaines, L., & Abbott, A. P. (2020). The importance of design in lithium ion battery recycling - a critical review. *Green Chemistry : An International Journal and Green Chemistry Resource : GC, 22*(22), 7585–763. 10.1039/d0gc02745f

Tiwari, S. K., Pande, S., Agrawal, S., & Bobade, S. M. (2015). Selection of selective laser sintering materials for different applications. *Rapid Prototyping Journal, 21*(6), 630–648. 10.1108/RPJ-03-2013-0027

U.S. Mineral Commodity Summaries (2024). Retrieved 24.1.2025, from https://pubs.usgs.gov/periodicals/mcs2024/mcs2024-lithium.pdf

US Geological Survey, & Statista. (2024a). Major countries in worldwide lithium mine production in 2023.

US Geological Survey, & Statista. (2024b). Mine production of lithium worldwide from 2010 to 2023.

Velazquez, L., & Muhr, H. (2025). Lithium recovery from secondary sources: A review in battery recycling with emphasis on chemical precipitation. *Comptes Rendus.Chimie, 27*, 1–9. 10.5802/crchim.316

Virolainen, S. (2013). *Hydrometallurgical recovery of valuable metals from secondary raw materials*

Wang, S., Li, P., Cui, W., Zhang, H., Wang, H., Zheng, S., & Zhang, Y. (2016). Hydrothermal synthesis of lithium-enriched β-Li 2 TiO 3 with an ion-sieve application: excellent lithium adsorption. *RSC Advances, 6*(104), 102608–102616. 10.1039/C6RA18018C

Weng, D., Duan, H., Hou, Y., Huo, J., Chen, L., Zhang, F., & Wang, J. (2020). Introduction of manganese based lithium-ion Sieve-A review. *Progress in Natural Science, 30*(2), 139–152. 10.1016/j.pnsc.2020.01.017

Weng, Y., Xu, S., Huang, G., & Jiang, C. (2013). Synthesis and performance of Li[(Ni1/3Co1/3Mn1/3)1−xMgx]O2 prepared from spent lithium ion batteries. *Journal of Hazardous Materials, 246-247*, 163–172. 10.1016/j.jhazmat.2012.12.028

Xu, X., Chen, Y., Wan, P., Gasem, K., Wang, K., He, T., Adidharma, H., & Fan, M. (2016). Extraction of lithium with functionalized lithium ion-sieves. *Progress in Materials Science, 84*, 276–313. 10.1016/j.pmatsci.2016.09.004

Xu, Z., Zhiyuan, L., Wenjun, M., & Qinxin, Z. (2023). Pretreatment options for the recycling of spent lithium-ion batteries: A comprehensive review. *Journal of Energy Storage, 72*, 108691. 10.1016/j.est.2023.108691

Yao, Y., Zhu, M., Zhao, Z., Tong, B., Fan, Y., & Hua, Z. (2018). Hydrometallurgical Processes for Recycling Spent Lithium-Ion Batteries: A Critical Review. *ACS Sustainable Chemistry & Engineering, 6*(11), 13611–13627. 10.1021/acssuschemeng.8b03545

Yu, J., Zhu, J., Luo, G., Chen, L., Li, X., Cui, P., Wu, P., Chao, Y., Zhu, W., & Liu, Z. (2023). 3D-printed titanium-based ionic sieve monolithic adsorbent for selective lithium recovery from salt lakes. *Desalination, 560*, 116651. 10.1016/j.desal.2023.116651

Zhang, L., Zhou, D., Yao, Q., & Zhou, J. (2016). Preparation of H2TiO3-lithium adsorbent by the sol–gel process and its adsorption performance. *Applied Surface Science, 368*, 82–87. 10.1016/j.apsusc.2016.01.203

Zhang, X., Bian, Y., Xu, S., Fan, E., Xue, Q., Guan, Y., Wu, F., Li, L., & Chen, R. (2018). Innovative Application of Acid Leaching to Regenerate Li(Ni 1/3 Co 1/3 Mn 1/3)O 2 Cathodes from Spent Lithium-Ion Batteries. *ACS Sustainable Chemistry & Engineering, 6*(5), 5959–5968. 10.1021/acssuschemeng.7b04373

Zhu, S., He, W., Li, G., Zhou, X., Zhang, X., & Huang, J. (2012). Recovery of Co and Li from spent lithium-ion batteries by combination method of acid leaching and chemical precipitation. *Transactions of Nonferrous Metals Society of China, 22*(9), 2274–2281. 10.1016/S1003-6326(11)61460-X